

Budgeted Multi-Objective Optimization with a Focus on the Central Part of the Pareto Front - Extended Version

David Gaudrie^{1,2}, Rodolphe le Riche², Victor Picheny³, Benoît Enaux¹, and
Vincent Herbert¹

¹Groupe PSA

²CNRS LIMOS, École Nationale Supérieure des Mines de Saint-Étienne

³INRA Toulouse

Abstract

Optimizing nonlinear systems involving expensive (computer) experiments with regard to conflicting objectives is a common challenge. When the number of experiments is severely restricted and/or when the number of objectives increases, uncovering the whole set of optimal solutions (the Pareto front) is out of reach, even for surrogate-based approaches. As non-compromising Pareto optimal solutions have usually little point in applications, this work restricts the search to relevant solutions that are close to the Pareto front center. The article starts by characterizing this center. Next, a Bayesian multi-objective optimization method for directing the search towards it is proposed. A criterion for detecting convergence to the center is described. If the criterion is triggered, a widened central part of the Pareto front is targeted such that sufficiently accurate convergence to it is forecasted within the remaining budget. Numerical experiments show how the resulting algorithm, C-EHI, better locates the central part of the Pareto front when compared to state-of-the-art Bayesian algorithms.

Keywords: Bayesian Optimization, Computer Experiments, Multi-Objective Optimization

1 Introduction

Over the last decades, computer codes have been widely employed for optimal design. Practitioners measure the worth of a design with several criteria, which corresponds to a *multi-objective optimization* problem,

$$\min_{\mathbf{x} \in X} (f_1(\mathbf{x}), \dots, f_m(\mathbf{x})) \quad (1)$$

where $X \subset \mathbb{R}^d$ is the parameter space, and $f_j(\cdot)$, $j = 1, \dots, m$ are the m objective functions. Since these goals are generally competing, there does not exist a single solution \mathbf{x}^* minimizing every function in (1), but several *trade-off solutions* that are mutually *non-dominated* (ND). These solutions form the Pareto set \mathcal{P}_X , whose image corresponds to the Pareto front \mathcal{P}_Y .

Often, the f_j 's are outputs of a computationally expensive computer code (several hours to days for one evaluation), so that only a small number of experiments can be carried out. Under this restriction, Bayesian optimization methods [37, 30] have proven their effectiveness in single objective

problems. These techniques use a surrogate – generally a Gaussian Process (GP) [43, 49] – to the true function to locate the optimum. Extensions of Bayesian optimization to multi-objective cases have also been proposed, see [9, 33, 32, 19, 51, 42, 41]. In the case of extremely narrow budgets (say less than a hundred evaluations), obtaining an accurate approximation of the Pareto front is however out of reach, even for Bayesian approaches. This issue gets worse with increasing number of criteria. Looking for the whole front can anyway seem useless as the Pareto set will contain many *irrelevant* solutions from an end-user’s point of view.

In this paper, instead of trying to approximate the whole front, we search for a well-chosen part of it. Without any specific information about the preferences of the decision maker, we assume that *well-balanced* solutions are the most interesting ones. By specifically targeting them, we argue that convergence should be enhanced there.

Restricting the search to parts of the objective space has been widely discussed in evolutionary multi-objective optimization (e.g., [5, 17, 22]), and has also recently received attention in Bayesian multi-objective optimization (see Section 2.3 for a short review). Contrarily to existing multi-objective optimization techniques which guide the search using externally supplied information, in the current work, the preference region is automatically defined by processing GPs.

An overview of the proposed method, implemented through the C-EHI algorithm (for Centered Expected Hypervolume Improvement), is sketched in Figure 1. It uses the concept of Pareto front center that is defined in Section 3. C-EHI iterations are made of three steps. First, an estimation of the Pareto front center is carried out, as described in Section 3 and sketched in Figure 1a. Second, the estimated center allows to target well-balanced parts of the Pareto front by a modification of the EHI criterion (cf. Section 4). Figure 1b illustrates the idea. Third, to avoid wasting computations once the center is sufficiently well located, the part of the Pareto front that is searched for is broadened in accordance with the remaining budget. To this aim, a criterion to test convergence to the center is introduced in Section 5. When triggered (see Figure 1c), a new type of iteration starts until the budget is exhausted (see Figure 1d). Section 6 explains how the new goals are determined.

To assess the performance of the proposed methodology, a benchmark built from real-world airfoil aerodynamic data is used. It has variables in dimension $d = 3, 8$ and 22 that represent CAD parameters, and 2 to 4 aerodynamic objectives (lift and drag at different airfoil angles). These results are presented in Section 7. The default test case that illustrates the algorithm concepts before numerical testing (Figures 10 to 19) is the 2 objectives problem in 8 variables.

2 A brief review of Bayesian multi-objective optimization

2.1 Bayesian optimization

Bayesian optimization techniques [37] have become popular to tackle single-objective optimization problems within a limited number of iterations. These methods make use of Bayes rule: a prior distribution, usually a GP, is placed over f and is enhanced by observations to derive the posterior distribution. Denoting $Z(\cdot)$ the GP and $\mathcal{A}_n = \{(\mathbf{x}^1, y_1), \dots, (\mathbf{x}^n, y_n)\} = \{\mathbb{X}, \mathbb{Y}\}$ the observational event, the posterior GP conditioned on \mathcal{A}_n has a known Gaussian distribution:

$$\forall \mathbf{x} \in X, Y(\mathbf{x}) := [Z(\mathbf{x})|\mathcal{A}_n] \sim \mathcal{N}(\hat{y}(\mathbf{x}), s^2(\mathbf{x}))$$

where

$$\hat{y}(\mathbf{x}) = \hat{\mu} + k(\mathbf{x}, \mathbb{X})K^{-1}(\mathbb{Y} - \mathbf{1}\hat{\mu})$$

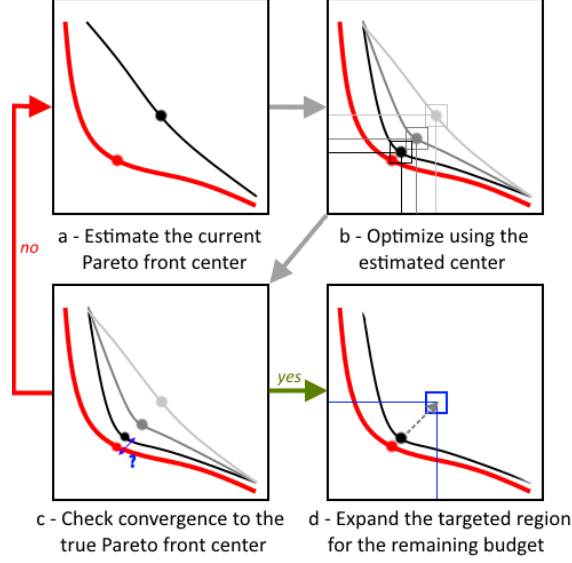


Figure 1: Sketch of the proposed C-EHI algorithm for targeting equilibrated solutions. The Pareto front center properties (a) are discussed in Section 3; How to guide the optimization with the center (b) is the topic of Section 4; Section 5 details how convergence to the true Pareto front center is tested (c); How to widen the search within the remaining budget (d), is presented in Section 6.

is the conditional mean function (a.k.a., the kriging mean predictor) [45, 43, 49, 46, 13] and

$$s^2(\mathbf{x}) = c(\mathbf{x}, \mathbf{x})$$

is the conditional variance, obtained from the conditional covariance function

$$c(\mathbf{x}, \mathbf{x}') = \widehat{\sigma}^2 \left(1 - k(\mathbf{x}, \mathbb{X}) K^{-1} k(\mathbb{X}, \mathbf{x}') + \frac{(1 - \mathbf{1}^\top K^{-1} k(\mathbf{x}, \mathbb{X}))(1 - \mathbf{1}^\top K^{-1} k(\mathbf{x}', \mathbb{X}))}{\mathbf{1}^\top K^{-1} \mathbf{1}} \right).$$

$K_{ij} = k(\mathbf{x}_i, \mathbf{x}_j)$ is the covariance matrix with $k(\cdot, \cdot)$ the covariance function (or kernel). $\widehat{\mu}$, $\widehat{\sigma}^2$ are the estimated mean and variance of the GP. $k(\cdot, \cdot)$ is typically chosen from a parametric family and its parameters are estimated, along with $\widehat{\mu}$ and $\widehat{\sigma}^2$ by likelihood maximization. Further discussion about these parameters and their estimation can be found e.g. in [43, 44].

Given a set of inputs $\mathbf{x}^{n+1}, \dots, \mathbf{x}^{n+s} \in X$, the posterior distribution of $Z(\cdot)$ at these points is a Gaussian vector

$$\begin{pmatrix} Y(\mathbf{x}^{n+1}) \\ \vdots \\ Y(\mathbf{x}^{n+s}) \end{pmatrix} \sim \mathcal{N} \left(\begin{pmatrix} \widehat{y}(\mathbf{x}^{n+1}) \\ \vdots \\ \widehat{y}(\mathbf{x}^{n+s}) \end{pmatrix}, \Gamma \right),$$

with $\Gamma_{a,b} = c(\mathbf{x}^a, \mathbf{x}^b)$. It is possible to simulate plausible values of $f(\cdot)$ by sampling n_{sim} GPs $\widetilde{Y}^{(k)}(\cdot)$, $k = 1, \dots, n_{sim}$ at $\mathbf{x}^{n+1}, \dots, \mathbf{x}^{n+s} \in X$. GP simulations require the Cholesky decomposition of the $s \times s$ matrix Γ and are therefore only tractable for moderate sample sizes.

For optimization purposes, new data points $(\mathbf{x}^{n+1}, f(\mathbf{x}^{n+1}))$ are sequentially sampled through the maximization of an *acquisition function* (or infill criterion) until a limiting number of function

evaluations, the *budget*, is attained. Acquisition functions use the posterior distribution $Y(\cdot)$. A commonly used infill criterion is the Expected Improvement (EI) [37, 28], which balances minimization of the GP mean (“exploitation” of past information) and maximization of the GP variance (“exploration” of new regions of the design space) in order to both search for the minimum of $f(\cdot)$ and improve the GP accuracy. The Expected Improvement below a threshold T is defined as

$$\text{EI}(\mathbf{x}; T) := \mathbb{E}[(T - Z(\mathbf{x}))_+ | \mathcal{A}_n] \quad (2)$$

which is computable in closed-form:

$$\text{EI}(\mathbf{x}; T) = (T - \hat{y}(\mathbf{x}))\phi\left(\frac{T - \hat{y}(\mathbf{x})}{s(\mathbf{x})}\right) + s(\mathbf{x})\varphi\left(\frac{T - \hat{y}(\mathbf{x})}{s(\mathbf{x})}\right) \quad (3)$$

φ and ϕ correspond to the probability density function and to the cumulative distribution function of a standard normal random variable, respectively. T is generally set as the best value observed so far, $f_{\min} := \min(y_1, \dots, y_n)$. EGO iteratively evaluates the function to optimize at the EI maximizer (Figure 2) before updating the GP. During the update step, the covariance parameters are re-estimated and the additional evaluation taken into account, which modifies the conditional mean and covariance. At the end of the procedure, the best observed design and its performance, $\mathbf{x}^* := \arg \min_{i=1, \dots, \text{budget}} f(\mathbf{x}^i)$, $y^* := f(\mathbf{x}^*)$, are returned.

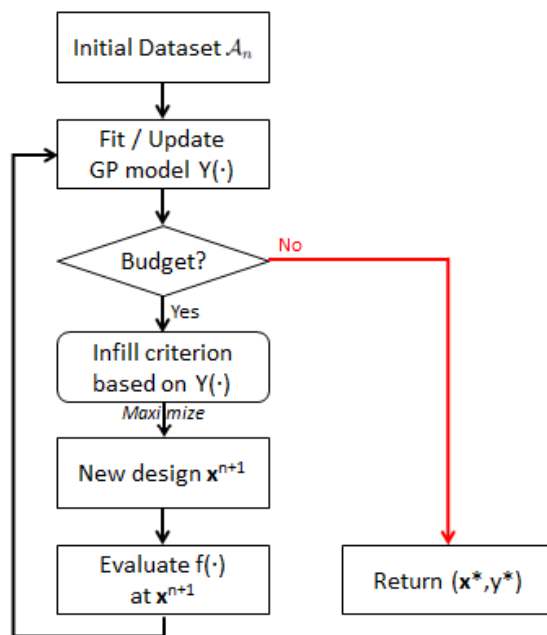


Figure 2: Outline of a Bayesian optimization algorithm

2.2 Extension to the multi-objective case

In the multi-objective case, there does not exist one single solution to the optimization problem. Instead, the solution of (1) is a (possibly infinite) set of optimal solutions, called the Pareto set $\mathcal{P}_{\mathcal{X}}$.

Designs in $\mathcal{P}_{\mathcal{X}}$ correspond to an optimal compromise in the sense that it is not possible to find a competitor being better in all objectives simultaneously.

Mathematically, $\mathcal{P}_{\mathcal{X}} = \{\mathbf{x} \in X : \nexists \mathbf{x}' \in X, \mathbf{f}(\mathbf{x}') \preceq \mathbf{f}(\mathbf{x})\}$ where \preceq stands for Pareto domination in \mathbb{R}^m as $\mathbf{f}(\mathbf{x}) := (f_1(\mathbf{x}), \dots, f_m(\mathbf{x}))^\top$ is no longer a scalar, but an m -dimensional objective vector. The Pareto front $\mathcal{P}_{\mathcal{Y}}$ is the image of the Pareto set and contains only non-dominated solutions: $\mathcal{P}_{\mathcal{Y}} = \mathbf{f}(\mathcal{P}_{\mathcal{X}}) = \{\mathbf{y} \in Y : \nexists \mathbf{y}' \in Y, \mathbf{y}' \preceq \mathbf{y}\}$, with $Y = \mathbf{f}(X) \subset \mathbb{R}^m$ the image of the design space through the objectives. Multi-objective optimizers aim at finding an approximation front built upon past observations $\widehat{\mathcal{P}}_{\mathcal{Y}} = \{\mathbf{y} \in \mathbb{Y} : \nexists \mathbf{y}' \in \mathbb{Y}, \mathbf{y}' \preceq \mathbf{y}\}$ to $\mathcal{P}_{\mathcal{Y}}$, with some properties such as convergence or diversity. Evolutionary Multi-Objective Optimization Algorithms (EMOA) have proven their benefits for solving Multi-Objective Problems [14]. They are however not adapted to expensive objectives.

Multi-objective extensions to EGO do exist. These Bayesian approaches generally model the objective functions $f_j(\cdot)$ as independent GP's $Y_j(\cdot)$. Svensson [50] has considered the GP's to be (negatively) correlated in a bi-objective case, without noticing significant benefits. The GP framework enables prediction of the objective functions, $\widehat{y}_j(\mathbf{x})$ and the uncertainty related to it, $s_j^2(\mathbf{x})$, $\forall \mathbf{x} \in X$. As for the single-objective case, an acquisition function is used for determining $\mathbf{x}^{t+1} \in X$, the most promising next iterate to be evaluated. In some approaches, the m surrogates are aggregated or use an aggregated form of EI [33, 27, 36, 57]. Other methods use a multi-objective infill criterion, for taking the simultaneous knowledge of all metamodels into account [52]. EHI [19, 18, 20], EMI [50, 51], and Keane's Euclidean-based Improvement [32] are three multi-objective infill criteria that reduce to EI when facing a single objective. SMS [42] is based on a lower confidence bound strategy, and SUR [41] considers the stepwise uncertainty reduction on the Pareto front. These infill criteria aim at providing new non-dominated points and eventually approximating the Pareto front in its entirety. The outline of these methods is the same as in Figure 2, excepted that m surrogates $Y_1(\cdot), \dots, Y_m(\cdot)$ and m objective functions are now considered, and that an empirical Pareto set $\widehat{\mathcal{P}}_{\mathcal{X}}$ and Pareto front $\widehat{\mathcal{P}}_{\mathcal{Y}}$ are returned.

EHI: a multi-objective optimization infill criterion

EHI [19, 18, 20] is one of the most competitive [55] multi-objective infill criterion. It rewards the expected growth of the Hypervolume Indicator [58], corresponding to the hypervolume dominated by the approximation front up to a reference point \mathbf{R} (see Fig. 3), when adding a new observation \mathbf{x} . More precisely, the Hypervolume Indicator of a set \mathcal{A} is

$$H(\mathcal{A}; \mathbf{R}) = \bigcup_{\mathbf{y} \in \mathcal{A}} \int_{\mathbf{y} \preceq \mathbf{z} \preceq \mathbf{R}} d\mathbf{z} = \Lambda \left(\bigcup_{\mathbf{y} \in \mathcal{A}} \{\mathbf{z} : \mathbf{y} \preceq \mathbf{z} \preceq \mathbf{R}\} \right)$$

where Λ is the Lebesgue measure on \mathbb{R}^m . The Hypervolume Improvement induced by $\mathbf{y} \in \mathbb{R}^m$ is $I_H(\mathbf{y}; \mathbf{R}) = H(\mathcal{A} \cup \{\mathbf{y}\}; \mathbf{R}) - H(\mathcal{A}; \mathbf{R})$. In particular, if $\mathcal{A} \preceq \mathbf{y}$ (in the sense that $\exists \mathbf{a} \in \mathcal{A} : \mathbf{a} \preceq \mathbf{y}$), or if $\mathbf{y} \not\preceq \mathbf{R}$, $I_H(\mathbf{y}; \mathbf{R}) = 0$. For a design \mathbf{x} , EHI($\mathbf{x}; \mathbf{R}$) is

$$\text{EHI}(\mathbf{x}; \mathbf{R}) := \mathbb{E}[I_H(\mathbf{Y}(\mathbf{x}); \mathbf{R})] \quad (4)$$

The Hypervolume Indicator being a refinement of the Pareto dominance [19, 52] ($\mathcal{A} \preceq \mathcal{B} \Rightarrow H(\mathcal{A}; \mathbf{R}) > H(\mathcal{B}; \mathbf{R})$ for two non-dominated sets \mathcal{A} and \mathcal{B} , and any reference point \mathbf{R}), and as the Hypervolume Improvement induced by a dominated solution equals zero, EHI maximization

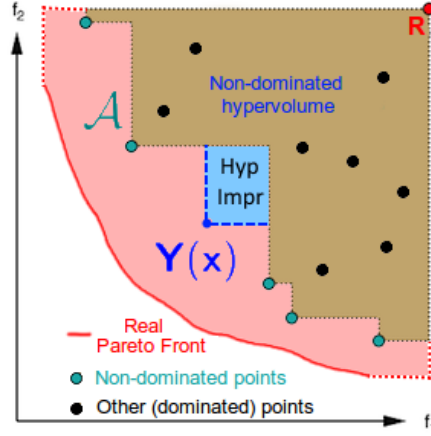


Figure 3: The Hypervolume Indicator of the non-dominated set (green points) corresponds to the area dominated by it, up to \mathbf{R} (in brown). The blue rectangle is the hypervolume improvement brought by $\mathbf{Y}(\mathbf{x})$, $I_H(\mathbf{Y}(\mathbf{x}); \mathbf{R})$.

intrinsically leads to Pareto optimality. It also favors well-spread solutions, as the hypervolume increase is small when adding a new value close to an already observed one in the objective space [3, 4].

Several drawbacks should be mentioned. First, the expensive computation of an m -dimensional hypervolume, relying on Monte-Carlo methods for $m > 2$ is required. Even if new efficient approaches [54] have been proposed, it is costly with regard to other infill criteria used in multi-objective optimization and increases with m . Second, the Hypervolume Indicator is less relevant for many-objective optimization, as the amount of non-dominated solutions rises with m , and more and more solutions contribute to the growth of the non-dominated hypervolume. Last, the choice of the reference point \mathbf{R} is unclear and influences the optimization results, as will be discussed in Section 4.

2.3 Past work on targeted multi-objective optimization

Targeting special parts of the objective space has been largely discussed within evolutionary multi-objective optimization, see for example [5] or [35] for a review. Preference-based optimization makes use of user-supplied information concerning, among others, desired objective values, ranking of solutions or of objectives, in order to guide the search towards corresponding parts of the Pareto front.

Bayesian multi-objective optimization (see Section 2.2) most often relies on the EHI infill criterion where the Hypervolume is computed up to a reference point \mathbf{R} . \mathbf{R} has been originally thought as being a second order hyperparameter with default values chosen so that all Pareto optimal points are valued in the EHI. For example, several studies (e.g. [42]) suggest taking $\mathbf{N} + 1$ (\mathbf{N} being the Nadir point of the empirical Pareto front).

Later, the effect of \mathbf{R} has received some attention. Auger et al. [3, 4] have theoretically and experimentally investigated the μ -optimal distribution on the Pareto front induced by the choice of

R. Ishibuchi et al. [26] have noticed a variability in the solutions given by an EMO algorithm when **R** changes. Feliot [21] has also observed that **R** impacts the approximation front and recommends **R** to be neither too far away nor too close to \mathcal{P}_Y . By calculating EHI restricted to areas dominated by “goal points”, Parr [40] implicitly acted on **R** and noticed fast convergence when the goal points were taken on $\widehat{\mathcal{P}}_Y$.

Previous works in Bayesian Multi-Objective Optimization have also targeted particular areas of the objective space thanks to ad-hoc infill criteria. The Weighted expected Hypervolume Improvement (WHI) [59, 1, 2, 10] is a variant of EHI that emphasizes given parts of the objective space through a user-defined weighting function. In [56, 53], the Truncated EHI criterion is studied where the Gaussian distribution is restricted to a user-supplied hyperbox in which new solutions are sought.

The algorithm proposed here targets a specific part of the Pareto front, its center, through a choice of **R** that is no longer arbitrarily chosen.

3 Center of the Pareto front: definition and estimation

3.1 Definitions

To the best of our knowledge, no formal definition of the center of a Pareto front exists. We are interested in a point that “visually” corresponds to an equilibrium among all objectives, within non-dominated points. Before defining the center of a Pareto front, other concepts of multi-objective optimization have to be outlined.

Definition 3.1. The *Ideal point* **I** of a Pareto front \mathcal{P}_Y is its component-wise minimum, $\mathbf{I} = (\min_{\mathbf{y} \in \mathcal{P}_Y} y_1, \dots, \min_{\mathbf{y} \in \mathcal{P}_Y} y_m)$.

The Ideal point also corresponds to the vector composed of each objective function minimum. Obviously, there exists no **y** better in *all* objectives than the minimizer of objective *j*. As a consequence, the latter belongs to \mathcal{P}_Y and $\min_{\mathbf{y} \in \mathcal{P}_Y} y_j = \min_{\mathbf{y} \in Y} y_j$, $j = 1, \dots, m$. **I** can therefore be alternatively defined as $(\min_{\mathbf{x} \in X} f_1(\mathbf{x}), \dots, \min_{\mathbf{x} \in X} f_m(\mathbf{x}))$. The decomposition on each objective does not hold for the Nadir point, which depends on the Pareto front structure:

Definition 3.2. The *Nadir point* **N** of a Pareto front \mathcal{P}_Y is the component-wise maximum of the Pareto front, $\mathbf{N} = (\max_{\mathbf{y} \in \mathcal{P}_Y} y_1, \dots, \max_{\mathbf{y} \in \mathcal{P}_Y} y_m)$.

I and **N** are virtual points, that is to say that there generally does not exist an $\mathbf{x} \in X$ such that $\mathbf{f}(\mathbf{x}) = \mathbf{I}$ or **N**. They are *bounding* points for the Pareto front, as every $\mathbf{y} \in \mathcal{P}_Y$ will be contained in the hyperbox defined by these points.

Definition 3.3. An *extreme point* for the *j*-th objective, $\boldsymbol{\nu}^j$, is an *m*-dimensional vector that belongs to the Pareto front, $\boldsymbol{\nu}^j \in \mathcal{P}_Y$, and such that $\nu_j^j = N_j$. The Nadir point can thus be rewritten as $\mathbf{N} = (\nu_1^1, \dots, \nu_m^m)$. A *j*-th extreme design point is $\boldsymbol{\xi}^j \in X$ such that $\mathbf{f}(\boldsymbol{\xi}^j) = \boldsymbol{\nu}^j$.

In the following, extreme points of the approximation front $\widehat{\mathcal{P}}_Y$ are denoted by $\widehat{\boldsymbol{\nu}}^j$, hence the Nadir of that empirical front is $\widehat{\mathbf{N}} = (\widehat{\nu}_1^1, \dots, \widehat{\nu}_m^m)$. Note that we will also introduce in Section 3.3 the notation $\widehat{\mathbf{N}}$ to denote an estimator of the Nadir point.

We can now define the center of a Pareto front:

Definition 3.4. The center of a Pareto front \mathbf{C} is the closest point in Euclidean distance to \mathcal{P}_Y on the Ideal-Nadir line \mathcal{L} .

In the field of Game Theory, our definition of the center of a Pareto front corresponds to a particular case of the Kalai-Smorodinsky equilibrium [31], taking the Nadir as disagreement point $\mathbf{d} \equiv \mathbf{N}$. This equilibrium aims at equalizing the ratios of maximal gains of the players, which is the appealing property for the center of a Pareto front.

In the case where the Pareto front is an m -dimensional continuous hypersurface, \mathbf{C} corresponds to the intersection between \mathcal{P}_Y and \mathcal{L} . In a more general case, e.g. if the Pareto front is not continuous, or contains some lower dimensional hypersurfaces, \mathbf{C} is the projection of the closest point belonging to \mathcal{P}_Y on \mathcal{L} . The computation of this point remains cheap even for a large m in comparison with alternative definitions involving e.g. the computation of a barycenter in high-dimensional spaces. Some examples for two-dimensional fronts are shown in Figure 4. The center of the Pareto front has also some nice properties that are detailed in following section.

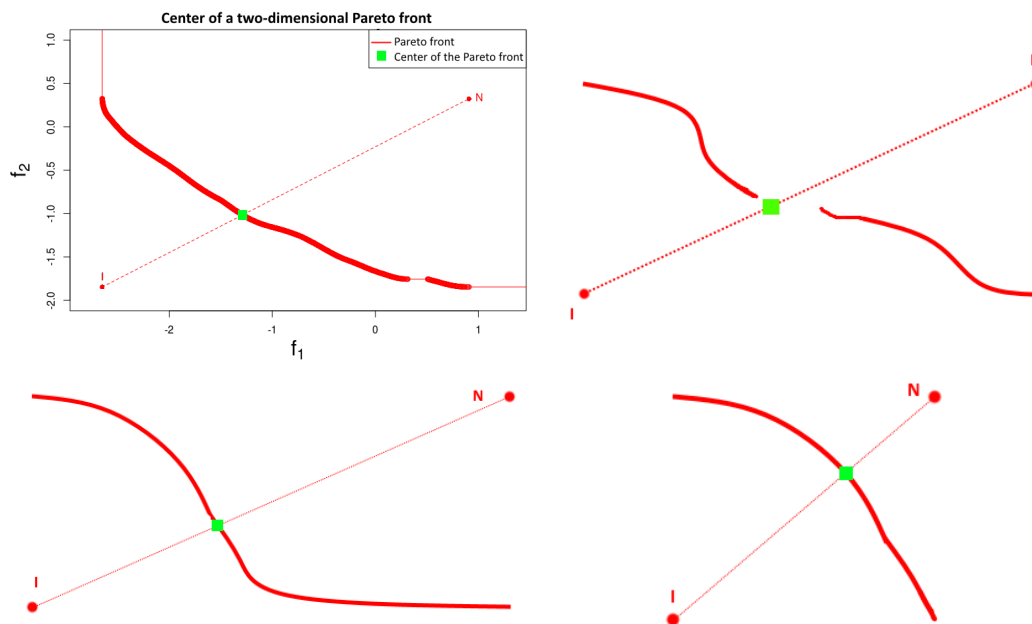


Figure 4: Examples of two-dimensional Pareto fronts and their center. Notice that on the bottom, the left and the right fronts are the same, except that the left is substantially extended in the x direction. However, the center has been only slightly modified.

3.2 Properties

Invariance to a linear scaling of the objectives

The Kalai-Smordinsky solution has been proved to verify a couple of properties, such as invariance to linear scaling¹ [31], which hold in our case. We extend here the linear invariance to the case where there is no intersection between \mathcal{P}_Y and \mathcal{L} .

Proposition 1 (Center invariance to linear scaling, intersection case). When \mathcal{P}_Y intersects \mathcal{L} , the intersection is unique and is the center of the Pareto front. Furthermore, in that case, the center is invariant after a linear scaling $S : \mathbb{R}^m \rightarrow \mathbb{R}^m$ of the objectives: $S(\mathbf{C}(\mathcal{P}_Y)) = \mathbf{C}(S(\mathcal{P}_Y))$.

Proof. First, it is clear that if \mathcal{P}_Y intersects \mathcal{L} , the intersection is unique. Indeed, as in non degenerated cases $\mathbf{I} \prec \mathbf{N}$, $t\mathbf{I} + (1-t)\mathbf{N} \prec t'\mathbf{I} + (1-t')\mathbf{N} \Leftrightarrow t > t'$. Two points on \mathcal{L} are different as long as $t \neq t'$. \mathcal{P}_Y being only composed of non-dominated points it is impossible to find two different points $t\mathbf{I} + (1-t)\mathbf{N}$ and $t'\mathbf{I} + (1-t')\mathbf{N}$ that belong simultaneously to \mathcal{P}_Y . Obviously, as it lies on \mathcal{L} , $\nexists \mathbf{y} \in \mathcal{P}_Y$ that is closer to it.

Let \mathbf{C} be this intersection. S being a linear scaling, it can be expressed in the form $S(\mathbf{y}) = \mathbf{A}\mathbf{y} + \mathbf{b}$ with \mathbf{A} an $m \times m$ diagonal matrix with entries $a_i > 0$, and $\mathbf{b} \in \mathbb{R}^m$. Applying this scaling to the objective space modifies \mathbf{C} to $\mathbf{C}' = \mathbf{A}\mathbf{C} + \mathbf{b}$, \mathbf{I} to $\mathbf{I}' = \mathbf{A}\mathbf{I} + \mathbf{b}$ and \mathbf{N} to $\mathbf{N}' = \mathbf{A}\mathbf{N} + \mathbf{b}$. Because the scaling preserves orderings of the objectives, \mathbf{C}' remains non-dominated, and \mathbf{I}' and \mathbf{N}' remain the Ideal point and the Nadir point of \mathcal{P}_Y in the scaled objective space. As \mathbf{C} belongs to \mathcal{L} it writes $t\mathbf{I} + (1-t)\mathbf{N}$ for one $t \in [0, 1]$, and therefore

$$\begin{aligned} \mathbf{C}' &= \mathbf{A}(t\mathbf{I} + (1-t)\mathbf{N}) + \mathbf{b} \\ &= t\mathbf{A}\mathbf{I} + (1-t)\mathbf{A}\mathbf{N} + \mathbf{b} \\ &= t(\mathbf{A}\mathbf{I} + \mathbf{b}) + (1-t)(\mathbf{A}\mathbf{N} + \mathbf{b}) \\ &= t\mathbf{I}' + (1-t)\mathbf{N}' \end{aligned}$$

\mathbf{C}' is thus the unique point belonging to both the Pareto front and to the Ideal-Nadir line in the transformed objective space: it is the center in the scaled objective space. \square

In the bi-objective case ($m = 2$), we also show that a linear scaling applied to the objective space does not change the order of Euclidean distances to \mathcal{L} . When $\mathcal{P}_Y \cap \mathcal{L} = \emptyset$, the closest $\mathbf{y} \in \mathcal{P}_Y$ to \mathcal{L} , whose projection on \mathcal{L} produces \mathbf{C} , remains the closest after any linear scaling of the objective space.

Proposition 2 (Center invariance to linear scaling, 2D case). Let $\mathbf{y}, \mathbf{y}' \in Y \subset \mathbb{R}^2$, and \mathcal{L} be a line in \mathbb{R}^2 passing through the two points \mathbf{I} and \mathbf{N} . Let $\Pi_{\mathcal{L}}$ be the projection on \mathcal{L} . If $\|\mathbf{y} - \Pi_{\mathcal{L}}(\mathbf{y})\| \leq \|\mathbf{y}' - \Pi_{\mathcal{L}}(\mathbf{y}')\|$, then \mathbf{y} remains closer to \mathcal{L} than \mathbf{y}' after having applied a linear scaling $S : \mathbb{R}^2 \rightarrow \mathbb{R}^2$ to Y .

Proof. Let A be the area of the $\mathbf{I}\mathbf{y}\mathbf{N}$ triangle and A' be the area of $\mathbf{I}\mathbf{y}'\mathbf{N}$. Applying a linear scaling $S(\mathbf{y}) = \mathbf{A}\mathbf{y} + \mathbf{b}$ with $\mathbf{A} = \begin{pmatrix} \alpha & 0 \\ 0 & \beta \end{pmatrix}$, $\alpha, \beta > 0$ to Y will modify the areas A and A' by the same

¹ in Game Theory, given a feasible agreement set $F \subset \mathbb{R}^m$ (Y in our context) and a disagreement point $\mathbf{d} \in \mathbb{R}^m$ (\mathbf{N} here), a KS solution $f \in F$ (the center \mathbf{C}) satisfies the four following requirements: Pareto optimality, symmetry with respect to the objectives, invariance to affine transformations (proven in Proposition 1) and, contrarily to a Nash solution, monotonicity with respect to the number of possible agreements in F .

factor $\alpha\beta$. Thus, $\|S(\mathbf{y}) - \Pi_{S(\mathcal{L})}(S(\mathbf{y}))\| \leq \|S(\mathbf{y}') - \Pi_{S(\mathcal{L})}(S(\mathbf{y}'))\|$ still holds: in the transformed subspace, \mathbf{y} remains closer to \mathcal{L} than \mathbf{y}' , as illustrated in Figure 5 \square

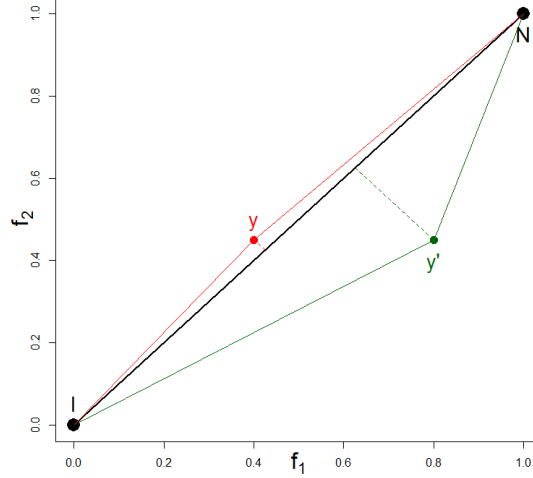


Figure 5: Applying any linear scaling to f_1 and f_2 will multiply the area of both triangles by the same factor. As a consequence, linear scaling does not modify the closest point to \mathbf{IN} .

This property is of interest as the solutions in the approximation front $\widehat{\mathcal{P}}_{\mathcal{Y}}$ will generally not belong to \mathcal{L} . Applying a linear scaling to Y in a bi-objective case does not change the solution in $\widehat{\mathcal{P}}_{\mathcal{Y}}$ that generates $\widehat{\mathbf{C}}$. However, exceptions may occur for $m \geq 3$ as the closest $\mathbf{y} \in \mathcal{P}_{\mathcal{Y}}$ to \mathcal{L} may not remain the same after a particular affine transformation of the objectives, as seen in the following example:

Let us consider the case of an approximation front composed of the five following non-dominated

points (in rows), in a three-dimensional space: $\mathbf{P} = \begin{bmatrix} 1 & 0 & 0 \\ 0 & 1 & 0 \\ 0 & 0 & 1 \\ 0.5 & 0.5 & 0.6 \\ 0.5 & 0.55 & 0.5 \end{bmatrix}$. The Ideal point is $\mathbf{I} =$

$(0, 0, 0)^{\top}$ and the Nadir point $\mathbf{N} = (1, 1, 1)^{\top}$. The squared Euclidean distance to \mathcal{L} of these 5 points equals respectively $2/3$, $2/3$, $2/3$, $0.02/3$ and $0.005/3$, hence $\mathbf{P}^5 = (0.5, 0.55, 0.5)^{\top}$ is the closest

point to \mathcal{L} . Let us now apply a linear scaling $S(\mathbf{y}) = \mathbf{A}\mathbf{y}$ with $\mathbf{A} = \begin{pmatrix} 3 & 0 & 0 \\ 0 & 3 & 0 \\ 0 & 0 & 1 \end{pmatrix}$. In the modified

objective space, we now have $\tilde{\mathbf{P}} = \begin{bmatrix} 3 & 0 & 0 \\ 0 & 3 & 0 \\ 0 & 0 & 1 \\ 1.5 & 1.5 & 0.6 \\ 1.5 & 1.65 & 0.5 \end{bmatrix}$, $\tilde{\mathbf{I}} = (0, 0, 0)^{\top}$ and $\tilde{\mathbf{N}} = (3, 3, 1)^{\top}$. The squared

distances to $\tilde{\mathcal{L}}$ after scaling are now respectively $1710/361$, $1710/361$, $342/361$, $3.42/361$, $4.275/361$. After scaling, the fourth point becomes the closest to the line. As the projection of the latter on

\mathcal{L} is different from the projection of the fifth point, the center of the Pareto front will change after this scaling.

Low sensitivity to Ideal and Nadir variations

Another positive property is the low sensitivity of \mathbf{C} with regard to extreme points. This property is appealing because the Ideal and the Nadir will be estimated with errors at the beginning of the search (cf. Section 3.3) and having a stable target \mathbf{C} prevents dispersing search efforts.

Under mild assumptions, the following Proposition expresses the low sensitivity in terms of the norm of the gradient of \mathbf{C} with respect to \mathbf{N} . Before, Lemma 1 gives a condition on the normal vector to the Pareto front that will be needed to prove the Proposition.

Lemma 1. Let $\mathbf{y}^* \in \mathbb{R}^m$ be a Pareto optimal solution, and the Pareto front be continuous and differentiable at \mathbf{y}^* with $\mathbf{d} \in \mathbb{R}^m$ the normal vector to the Pareto front at \mathbf{y}^* . Then all components of \mathbf{d} have the same sign.

Proof. Because of the differentiability assumption at \mathbf{y}^* and the definition of Pareto dominance, \mathbf{d} cannot have null components. Suppose that some components in \mathbf{d} have opposite signs, \mathbf{d}^+ corresponding to positive ones and \mathbf{d}^- to negatives ones, $\mathbf{d} = [\mathbf{d}^+, \mathbf{d}^-]^\top$. Let ε^+ and ε^- be two small positive scalars such that $\frac{\varepsilon^+}{\varepsilon^-} = \frac{\sum_{i:d_i < 0} d_i^2}{\sum_{i:d_i > 0} d_i^2}$. Then, $\mathbf{f} = \mathbf{y}^* + \begin{pmatrix} -\varepsilon^+ \mathbf{d}^+ \\ \varepsilon^- \mathbf{d}^- \end{pmatrix}$ dominates \mathbf{y}^* and belongs to the local first order approximation to \mathcal{P}_Y since $\mathbf{d}^\top (\mathbf{f} - \mathbf{C}) = 0$, which is a contradiction as \mathbf{y}^* is Pareto optimal. \square

Proposition 3 (Stability of the Center to perturbations in Ideal and Nadir). Let \mathcal{P}_Y be locally continuous and $m - 1$ dimensional around its center \mathbf{C} . Then, $|\frac{\partial C_i}{\partial N_j}| < 1$, $i, j = 1, \dots, m$ where \mathbf{N} is the Nadir point, and the variation $\Delta \mathbf{C}$ of \mathbf{C} induced by a small variation $\Delta \mathbf{N}$ in \mathbf{N} verifies $\|\Delta \mathbf{C}\|_2 < \|\Delta \mathbf{N}\|_2$. A similar relation stands for small Ideal points variations, $\|\Delta \mathbf{C}\|_2 < \|\Delta \mathbf{I}\|_2$.

Proof. If \mathcal{P}_Y is locally continuous and $m - 1$ dimensional, \mathbf{C} is the intersection between \mathcal{L} and \mathcal{P}_Y . For simplicity, the Pareto front is scaled between 0 and 1, that is, $\mathbf{I} = \mathbf{0}_m$ and $\mathbf{N} = \mathbf{1}_m$. Proposition 1 ensures that the center is not modified by such a scaling. The tangent hyperplane to \mathcal{P}_Y at \mathbf{C} writes $\mathbf{d}^\top \mathbf{f} + e = 0$ where $\mathbf{d} \in \mathbb{R}^m$, the normal vector to the tangent hyperplane, and $e \in \mathbb{R}$ depend on \mathcal{P}_Y and are supposed to be known. Lemma 1 ensures that d_i , $i = 1, \dots, m$ have the same sign, that we choose positive. \mathbf{C} satisfies both $\mathbf{d}^\top \mathbf{C} = -e$ and $\mathbf{C} = (1 - \alpha_C)\mathbf{I} + \alpha_C \mathbf{N} = \alpha_C \mathbf{1}_m$ for some $\alpha_C \in]0, 1[$. Hence,

$$\mathbf{C} = \frac{-e}{\mathbf{d}^\top \mathbf{N}} \mathbf{N}, \quad C_i = \frac{-e}{\mathbf{d}^\top \mathbf{N}} N_i$$

$\forall j = 1, \dots, m, j \neq i,$

$$\frac{\partial C_i}{\partial N_j} = \frac{e N_i d_j}{(\mathbf{d}^\top \mathbf{N})^2} = \frac{-d_j}{\sum_k d_k N_k} C_i = \frac{-d_j}{\sum_k d_k} C_i$$

For $i = j$,

$$\frac{\partial C_i}{\partial N_i} = \frac{-e \mathbf{d}^\top \mathbf{N} + e N_i d_i}{(\mathbf{d}^\top \mathbf{N})^2} = \frac{C_i}{N_i} - \frac{C_i}{\sum_k d_k N_k} = C_i \left(1 - \frac{d_i}{\sum_k d_k} \right)$$

$C_i = \alpha_C \in]0, 1[\quad \forall i = 1, \dots, m$ and as the d_i 's share the same sign, $|d_i| \leq |\sum_k d_k|$. Therefore, $|\frac{\partial C_i}{\partial N_i}| < 1$ and $|\frac{\partial C_i}{\partial N_j}| < 1$. Consider now that \mathbf{N} is modified into $\mathbf{N} + \Delta \mathbf{N}$, which changes the center

to $\mathbf{C} + \Delta\mathbf{C}$. One has $\Delta\mathbf{C} = \nabla\mathbf{C} \cdot \Delta\mathbf{N}$ where $\nabla\mathbf{C}$ is the $m \times m$ matrix with entries $\frac{\partial C_i}{\partial N_j}$. Rearranging the terms of the derivatives into matrix form yields

$$\nabla\mathbf{C} = \alpha_C \left[I_m - \underbrace{\frac{1}{\sum_k d_k} \begin{pmatrix} d_1 & d_2 & \cdots & d_m \\ \vdots & \vdots & & \vdots \\ d_1 & d_2 & \cdots & d_m \end{pmatrix}}_D \right]$$

where I_m stands for the identity matrix here. D is a rank 1 matrix with positive entries whose rows sum to 1, and has eigenvalues 0 and 1 with respective multiplicity $m-1$ and 1. Consequently, $\nabla\mathbf{C}$'s largest eigenvalue is $\alpha_C \in]0, 1[$. Finally, $\|\Delta\mathbf{C}\|_2 \leq \|\nabla\mathbf{C}\|_2 \|\Delta\mathbf{N}\|_2 \leq \|\Delta\mathbf{N}\|_2$. By symmetry, the Proposition extends to the sensitivity of the center to the Ideal point, $|\frac{\partial C_i}{\partial I_j}| < 1$, $i, j = 1, \dots, m$ and $\|\Delta\mathbf{C}\|_2 < \|\Delta\mathbf{I}\|_2$. □

Remark 1. $\|\Delta\mathbf{C}\|_\infty$ considers the maximal \mathbf{C} variation in any direction. However, we have only found that $\|\Delta\mathbf{C}\|_\infty \leq 2\|\Delta\mathbf{N}\|_\infty$.

This less satisfactory result may be due to a too large upper bound. A few calculations lead to $\|I_m - D\|_\infty = \max(2 - 2d_1, \dots, 2 - 2d_m) = 2(1 - \min_{i=1, \dots, m} (d_i)) \leq 2$, hence $\|\nabla\mathbf{C}\|_\infty \leq 2$ and the final result. Even if a sharper upper bound would be desirable, it is interesting that whatever the front and the variation of \mathbf{N} , \mathbf{C} 's component-wise maximum variation is bounded by the component-wise \mathbf{N} maximum variation. Notice that the component which achieves the largest variation may not be the same for \mathbf{N} and for \mathbf{C} .

Proposition 3 is a local stability result. Without formal proof, it is observed that the center will be little affected by larger errors in Ideal and Nadir positions when compared to alternative definitions of the center. A typical illustration is as follows: the Nadir point is moved by a large amount in one objective (see Figure 6). The center is shifted by a relatively small amount and will continue to correspond to an area of equilibrium between *all* objectives. Other definitions of the center, typically those based on the barycenter of \mathcal{P}_Y would lead to a major displacement of \mathbf{C} . In Figure 6, the barycenter on \mathcal{P}_Y signaled by \mathbf{B} and \mathbf{B}' has $B'_2 \approx I_2$, which does not correspond to an equilibrated solution as the second objective would almost be at its minimum.

Example 1. Let us consider a continuous two-dimensional Pareto front \mathcal{P}_Y defined by $y_{PF}(x) = 1 - x^\alpha$ for $x \in [0, 1]$, and $\alpha > 0$. $\mathbf{I} = (0, 0)^\top$, $\mathbf{N} = (1, 1)^\top$ and $\mathbf{C} = (x_C, y_C)$ is the point verifying

$\begin{cases} y_C = x_C \\ y_C = 1 - x_C^\alpha \end{cases}$. For some particular values of α , an analytic solution \mathbf{C} can be obtained. Figure 7 shows a few fronts for different α 's. The intersection with the line spanning \mathbf{I} and \mathbf{N} is the center.

\mathbf{C} is a function of \mathcal{P}_Y and in particular of \mathbf{L} and \mathbf{R} , its extremes points determining \mathbf{I} and \mathbf{N} : $\mathbf{C} = f(\mathbf{L}, \mathbf{R})$. In the following, we analyze the behavior of \mathbf{C} when applying a slight modification to $\mathbf{R} = (x_R, y_R)$, which impacts \mathbf{I} and \mathbf{N} as $x_N = x_R$ and $y_I = y_R$. \mathbf{R} is transformed into $(x_R, -\varepsilon)$ for some small $\varepsilon > 0$ and a new $x_R > 1$, as in Figure 6. After this modification, $\mathbf{I} = (0, -\varepsilon)^\top$, $\mathbf{N} = (x_R, 1)^\top$ and \mathbf{C} verifies

$$\begin{cases} y = -\varepsilon + \frac{1 + \varepsilon}{x_R} x \\ y = 1 - x^\alpha \end{cases} \quad (5)$$

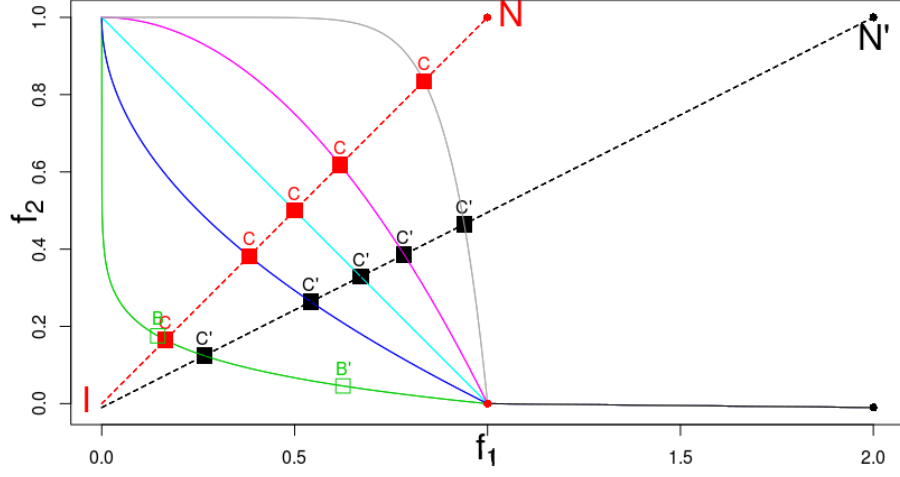


Figure 6: Illustration of the global stability of the center in 2D: adding the black part to the colored Pareto fronts will highly modify them and N' becomes the new Nadir point. The new center C' is relatively close to C despite this major N modification. B , a barycenter-based center would be much more affected, and would no longer correspond to an equilibrium.

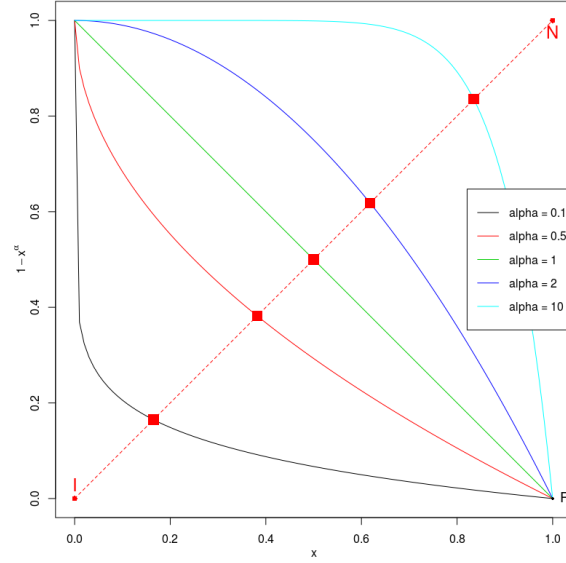


Figure 7: Pareto fronts and their center for five different values of α .

We assume that ε is small enough so that the intersection still takes place on the $1 - x^\alpha$ part of the front. Being interested in variations of C induced by the change of x_R , we compute $\frac{\partial x_C}{\partial x_R}$ and $\frac{\partial y_C}{\partial x_R}$. Using (5)

$$\frac{\partial y_C}{\partial x_R} = \frac{1+\varepsilon}{x_R} \frac{\partial x_C}{\partial x_R} - \frac{1+\varepsilon}{x_R^2} x_C = -\alpha \frac{\partial x_C}{\partial x_R} x_C^{\alpha-1} \quad (6)$$

Combining these equations

$$\frac{\partial x_C}{\partial x_R} \left[\frac{\alpha x_C^{\alpha-1} x_R}{x_R} + \frac{1+\varepsilon}{x_R} \right] = \frac{1+\varepsilon}{x_R} \frac{x_C}{x_R} = \frac{y_C + \varepsilon}{x_R}$$

as $y + \varepsilon = \frac{1+\varepsilon}{x_R} x_C$ using (5)'s first line,

$$\frac{\partial x_C}{\partial x_R} = \frac{y_C + \varepsilon}{\alpha x_C^{\alpha-1} x_R + 1 + \varepsilon} \xrightarrow{\varepsilon \rightarrow 0^+} \frac{y_C}{1 + \alpha x_C^{\alpha-1} x_R}$$

Since $\alpha > 0$, as well as x_C , y_C and x_R , $0 < \frac{\partial x_C}{\partial x_R} < 1$. We also notice a $\frac{1}{x_R}$ term, meaning that the displacement is reduced by the distance to \mathbf{R} .

Going back to the first equality in (6) and using again the remark,

$$\frac{\partial y_C}{\partial x_R} = \frac{1+\varepsilon}{x_R} \left[\frac{\partial x_C}{\partial x_R} - \frac{y_C + \varepsilon}{1+\varepsilon} \right] \xrightarrow{\varepsilon \rightarrow 0^+} \frac{1}{x_R} \left(\frac{\partial x_C}{\partial x_R} - y_C \right)$$

The previous calculation led us to $\frac{\partial x_C}{\partial x_R} \rightarrow \frac{y_C}{1 + \alpha x_C^{\alpha-1} x_R}$, so $\frac{\partial x_C}{\partial x_R} < y_C$. Therefore, $\frac{\partial y_C}{\partial x_R} < 0$ and this term is also damped by a $\frac{1}{x_R}$ factor. The multiplied quantities lying in $[0, 1]$, finally $-1 < \frac{\partial y_C}{\partial x_R} < 0$.

3.3 Estimation of the Pareto front center using Gaussian processes

Now that we have given a definition of \mathbf{C} relying on \mathcal{P}_Y through \mathbf{I} and \mathbf{N} , let us discuss the estimation of \mathbf{C} . The *real* front \mathcal{P}_Y is obviously unknown and at any stage of the algorithm, we solely have access to an approximation front $\widehat{\mathcal{P}}_Y$. The empirical Ideal and Nadir points (computed using $\widehat{\mathcal{P}}_Y$) could be weak estimates in the case of a biased approximation front. Thus, we propose an approach using the GPs $Y_j(\cdot)$ to better estimate \mathbf{I} and \mathbf{N} through conditional simulations.

Estimating \mathbf{I} and \mathbf{N} with GP simulations

Estimating the Ideal and the Nadir point accurately is a difficult task. Indeed, obtaining \mathbf{I} is equivalent to finding the minimum of each $f_j(\cdot)$, $j = 1, \dots, m$, which corresponds to m classical mono-objective optimization problems. Prior to computing \mathbf{N} , the whole Pareto front has to be unveiled but this is precisely our primary concern! Estimating \mathbf{N} before running the multi-objective optimization has been proposed in [15, 6] using modified EMOAs to emphasize extreme points. We aim at obtaining sufficiently accurate estimators $\widehat{\mathbf{I}}$ and $\widehat{\mathbf{N}}$ of \mathbf{I} and \mathbf{N} rather than solving these problems exactly. The low sensitivity of \mathbf{C} with regard to \mathbf{I} and \mathbf{N} discussed previously suggests that the estimation error should not be a too serious issue for computing \mathbf{C} . As seen in Section 2.1, given s simulation points $\mathbf{x}^{n+1}, \dots, \mathbf{x}^{n+s}$, possible responses at those locations can be obtained through the conditional GPs $Y_j(\cdot)$, $j = 1, \dots, m$. The simulated responses can be filtered by Pareto dominance to get n_{sim} simulated fronts $\widehat{\mathcal{P}}_Y^{(k)}$. The Ideal and Nadir points are then estimated by

$$\widehat{I}_j = \text{median}_{k=1, \dots, n_{sim}} \left(\min_{\mathbf{y} \in \widehat{\mathcal{P}}_Y^{(k)}} y_j \right); \widehat{N}_j = \text{median}_{k=1, \dots, n_{sim}} \left(\max_{\mathbf{y} \in \widehat{\mathcal{P}}_Y^{(k)}} y_j \right), j = 1, \dots, m.$$

Notice that the definition of \mathbf{I} is not based on the Pareto front. Hence the estimation of I_j does not require m -dimensional simulated fronts, but only single independently simulated responses $\widetilde{Y}_j^{(k)}$. By contrast, as the Nadir point needs the front to be defined, simulated fronts $\widetilde{\mathcal{P}}_Y^{(k)}$ are mandatory for estimating \mathbf{N} .

GP simulations are attractive for estimating extrema because they not only provide possible responses of the objective functions but also take into account the surrogate’s uncertainty. It would not be the case by applying a (multi-objective) optimizer to a deterministic surrogate such as the conditional mean functions. Even so, they rely on the choice of simulation points $\mathbf{x}^{n+i}, i = 1, \dots, s$ (in a d -dimensional space). For technical reasons (Cholesky or spectral decomposition of Γ_j required for sampling from the posterior), the number of points is restricted to $s \lesssim 5000$. \mathbf{x}^{n+i} have thus to be chosen in a smart way to make the estimation as accurate as possible. In order to estimate \mathbf{I} or \mathbf{N} , GP simulations are performed at \mathbf{x} ’s that have a great probability of contributing to one component of those points: first, the kriging mean and variance of a very large sample $\mathbb{S} \subset X$ is computed. The calculation of $\widehat{y}_j(\mathbb{S})$ and $s_j(\mathbb{S})$ is indeed tractable for large samples contrarily to GP simulations. Next, s designs are picked up from \mathbb{S} using these computations. In order to avoid losing diversity, the selection is performed using an importance sampling procedure [7], based on the probability of contributing to the components I_j or N_j .

As $I_j = \min_{\mathbf{x} \in X} f_j(\mathbf{x})$ good candidates are \mathbf{x} ’s such that $\mathbb{P}(Y_j(\mathbf{x}) < a_j)$ is large. To account for new evaluations of f_j , a typical value for a_j is the minimum observed value in the j -th objective, $\min_{i=1, \dots, n} f_j(\mathbf{x}^i)$. According to the surrogate, such points have the greatest probability of improving over the currently best value if they were evaluated.

Selecting candidates for estimating \mathbf{N} is more demanding. Indeed, as seen in Definition 3.2, N_j is not the maximum value over the whole objective space Y but over the unknown \mathcal{P}_Y , i.e., each N_j arises from a ND point. Thus the knowledge of an m -dimensional front is mandatory for estimating \mathbf{N} . The best candidates for \mathbf{N} ’s estimation are, by Definition 3.3, extreme design points. Quantifying which points are the most likely to contribute to the Nadir components, in other terms produce extreme points, is a more difficult task than its pendant for the Ideal. Good candidates are \mathbf{x} ’s such that the sum of probabilities $\mathbb{P}(Y_j(\mathbf{x}) > \widehat{v}_j^j, \mathbf{Y}(\mathbf{x}) \text{ ND}) + \mathbb{P}(\mathbf{Y}(\mathbf{x}) \preceq \widehat{\mathbf{v}}^j)$ is large. For reasons of brevity, the procedure is detailed in Appendix A.

Ideal-Nadir line and estimated center

To estimate \mathbf{I} and \mathbf{N} , we first select $s = 5000$ candidates from a large space-filling Design of Experiments (DoE) [24, 47], $\mathbb{S} \subset X$, with a density proportional to their probability of generating either a I_j or a N_j as discussed before. $s/2m$ points are selected for the estimation of each component of \mathbf{I} and \mathbf{N} . n_{sim} conditional GP simulations are then performed at those $\mathbf{x}^{n+i}, i = 1, \dots, s$ in order to generate simulated fronts, whose Ideal and Nadir points are aggregated through the medians to produce the estimated $\widehat{\mathbf{I}}$ and $\widehat{\mathbf{N}}$. The resulting simulated fronts are biased towards particular parts of the Pareto front (extreme points, individual minima).

Experiments have shown significant benefits over methodologies that choose \mathbf{x}^{n+i} ’s according to their probability of being not dominated by the whole approximation front, or that use s points from a space-filling DoE [39] in X . Figure 8 compares the component estimation of \mathbf{I} and \mathbf{N} for different techniques during one optimization run with $m = 3$ objectives. X.IN (blue curve) corresponds to

our methodology. The other curves stand for competing methodologies: X.LHS (green) selects the \mathbf{x}^{n+i} from a space-filling design, and X.ND (red) chooses them according to their probability of being non-dominated with respect to the entire front. NSGA-II (gold) does not select design points \mathbf{x}^{n+i} to perform GP simulations but rather uses the Ideal and Nadir point found by one run of the NSGA-II [16] multi-objective optimizer applied to the kriging predictors $\hat{y}_i(\cdot), i = 1, \dots, m$. The black dashed line corresponds to the component of the current empirical front, a computationally much cheaper estimator. The bold dashed line shows \mathbf{I} and \mathbf{N} 's true components.

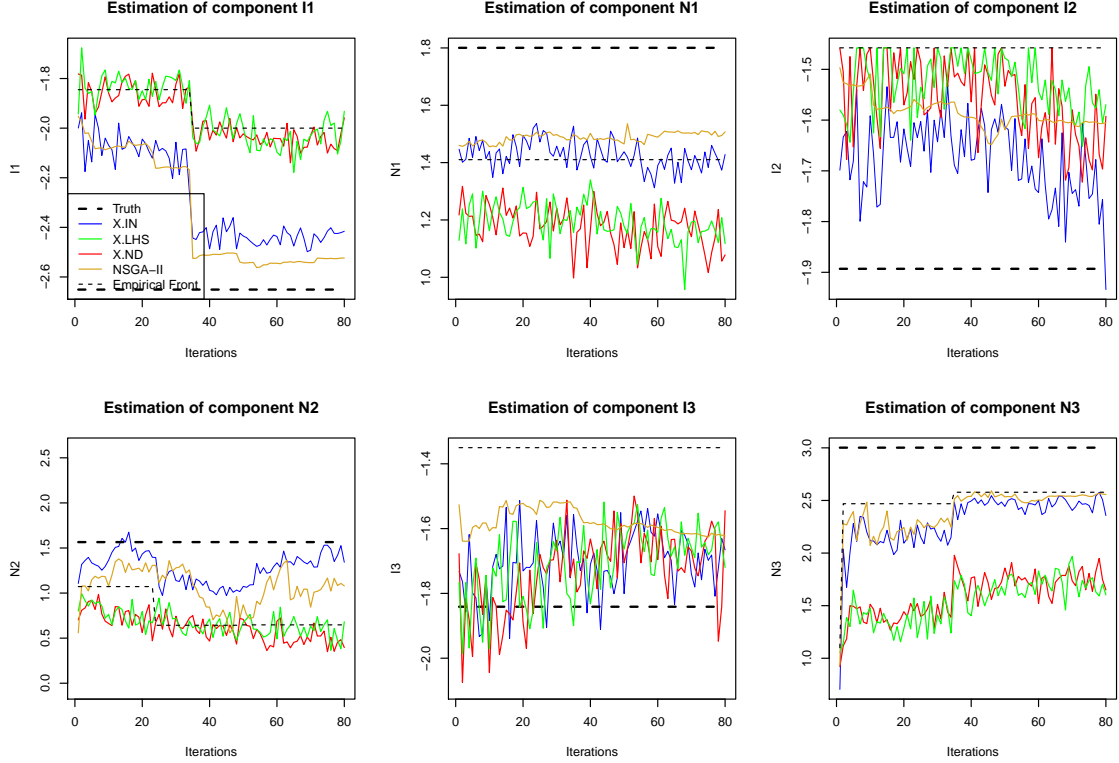


Figure 8: Example of estimation of \mathbf{I} and \mathbf{N} using different techniques. The proposed methodology (blue) is able to consistently produce close estimates to \mathbf{I} 's and \mathbf{N} 's components (bold black dashed line).

Our methodology outperforms the two other simulation techniques, because they do not perform the simulations specifically at locations that are likely to correspond to an extreme design point or to a single-objective minimizer. Benefits are also observed compared with the empirical Ideal and Nadir points, that are sometimes poor estimators (for example for I_1 , I_2 and N_2). Using the output of a multi-objective optimizer (here NSGA-II) applied to the kriging mean functions is also a promising approach but has the drawback of not considering any uncertainty in the surrogates (that may be large at the extreme parts of the Pareto front). It also suffers from classical EMOA's disadvantages, e.g. several runs would be required for more reliable results and convergence can

not be guaranteed. Note that as these methods rely on the surrogates they are biased by the earlier observations: the change of the empirical Ideal or Nadir point has an impact on the estimation. However, the X.IN, X.LHS and X.ND estimators compensate by considering the GPs uncertainty to reduce this bias.

As we are in fine not interested in the Ideal and the Nadir point but in the Pareto front center, we want to know if these estimations lead to a good $\hat{\mathbf{C}}$. Proposition 3 suggests that the small Ideal and Nadir estimation error should not be a too serious concern. This is confirmed by Figure 9, where the center estimation error is low with respect to the range of the Pareto front.

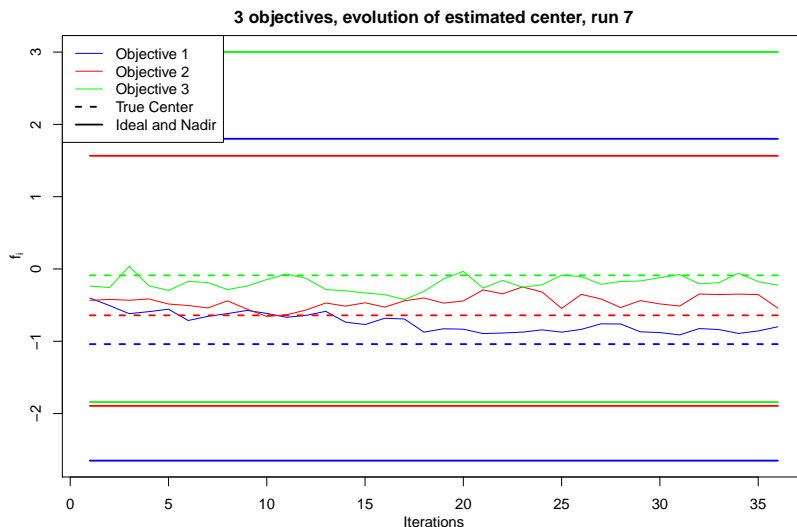


Figure 9: Evolution of the estimated center during one run (using $\hat{\mathbf{I}}$ and $\hat{\mathbf{N}}$ from Figure 8): $\hat{\mathbf{C}}$'s components are close to the true ones.

Figure 10 shows an example of one GP simulation targeting the extremes of the Pareto front. Notice the difference between the current empirical Pareto front (in blue) and the simulated front for \mathbf{N} and \mathbf{I} (in black): the extreme points which are simulated go well beyond those already observed.

Linearly extending the Pareto front approximation [25] and taking the intersection with $\hat{\mathcal{L}}$ was originally considered for defining $\hat{\mathbf{C}}$. But as an m -dimensional interpolated Pareto front is not necessarily composed of only $m - 1$ dimensional hyperplanes (but is a collection of polytopes of dimension at most $m - 1$), the intersection with an m -dimensional line does not necessarily exist.

4 An infill criterion to target the center of the Pareto front

4.1 Targeting the Pareto front center with the reference point

Our approach starts from the observation that any region of the objective space can be aimed targeted with EHI solely by controlling the reference point \mathbf{R} . Indeed, as $\mathbf{y} \not\leq \mathbf{R} \Rightarrow I_H(\mathbf{y}; \mathbf{R}) = 0$, the choice of \mathbf{R} is instrumental in deciding the combination of objectives for which improvement

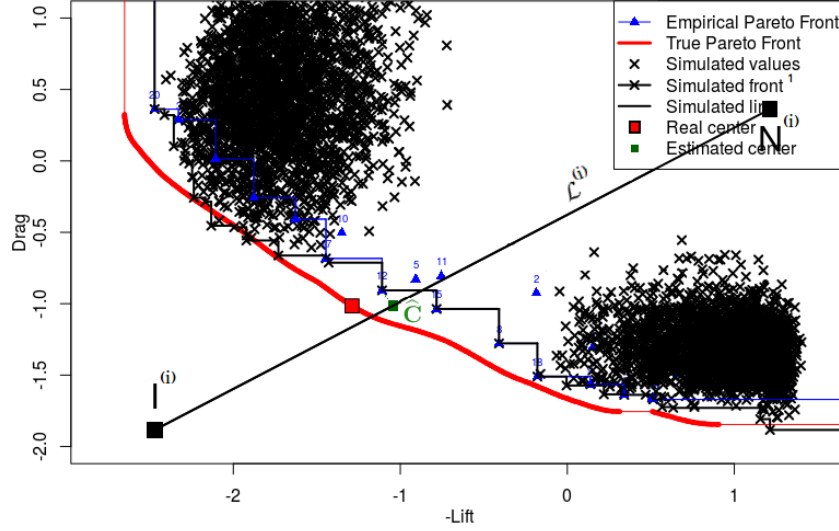


Figure 10: One GP simulation targeting the extremes of the Pareto front to enhance the estimation of \mathbf{I} and \mathbf{N} . The projection of the closest non-dominated point to \mathcal{L} on it is the estimated center (in green). The real center (in red) lies close to the estimated center and to the estimated Ideal-Nadir line.

occurs, the *improvement region*:

$$\mathcal{I}_{\mathbf{R}} := \{\mathbf{y} \in Y : \mathbf{y} \preceq \mathbf{R}\} .$$

As shown in Fig. 11, the choice of \mathbf{R} defines the region in objective space where $I_H > 0$ and where the maximum values of EHI are expected to be found. The choice of \mathbf{R} is crucial as it defines the region in objective space that is highlighted. To our knowledge, \mathbf{R} has always been chosen to be dominated by the whole approximation Front (that is, \mathbf{R} is at least the empirical Nadir point, which corresponds to the case of $\mathbf{R1}$ in Fig. 11). The targeting ability of \mathbf{R} can and should however be taken into account: for example, solutions belonging to the left part of the Pareto front in Fig. 11 can be aimed at using $\text{EHI}(\cdot; \mathbf{R2})$ instead of the more general $\text{EHI}(\cdot; \mathbf{R1})$.

Because of the extremely limited number of possible calls to the objective functions, we would like to prioritize the search by first looking for the Pareto front center. This is implemented simply by setting the reference point as the estimated center, $\mathbf{R} \equiv \hat{\mathbf{C}}$. Then, the algorithm maximizes $\text{EHI}(\mathbf{x}; \hat{\mathbf{C}})$ on \mathbf{x} . In contrast to other works that set \mathbf{R} at levels dominated by all Pareto optimal points, \mathbf{R} at $\hat{\mathbf{C}}$ will typically be non-dominated² since it is close to the empirical Pareto front.

$\hat{\mathbf{C}}$ corresponds to the center of the *current* approximation front, at a given moment t . Since the goal is to find optimal, better, solutions, it makes sense to look for points dominating it: at each iteration of the algorithm, after having estimated $\hat{\mathbf{C}}$, improvements over it are sought by maximizing $\text{EHI}(\cdot, \hat{\mathbf{C}})$.

²When using the projection of the closest non-dominated point on the line, exceptions may occur and $\hat{\mathbf{C}}$ may be dominated. In that case, it as to be slightly moved towards $\hat{\mathbf{I}}$.

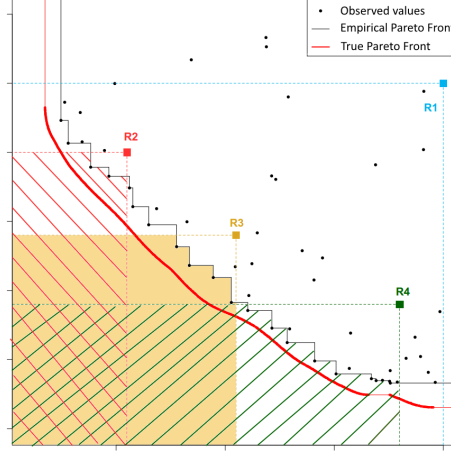


Figure 11: Different reference points and the areas $\mathcal{I}_{\mathbf{R}}$ that are targeted

4.2 mEI, a computationally efficient proxy to EHI

Choosing the Pareto front center, a non-dominated point, as reference point in EHI has an additional advantage: it allows to define a criterion that can replace EHI for targeted optimization at a much lower computational cost. We name this criterion mEI for multiplicative Expected Improvement.

Definition 4.1 (mEI criterion). The multiplicative Expected Improvement is the product of Expected Improvements in each objective defined in Equation (2)

$$\text{mEI}(\cdot; \mathbf{R}) := \prod_{j=1}^m \text{EI}_j(\cdot; R_j) . \quad (7)$$

mEI is a natural extension of the mono-objective Expected Improvement, as $(f_{\min} - \hat{y}(\mathbf{x}))_+$ is replaced by $\prod(\mathbf{R} - \hat{\mathbf{Y}}(\mathbf{x}))_+$.

mEI is an attractive infill criterion in several ways. First, it is able to target a part of the objective space via \mathbf{R} as the Improvement function it is built on differs from zero only in $\mathcal{I}_{\mathbf{R}}$. Conversely of course, as it does not take the shape of the current approximation front into account, mEI cannot help in finding well-spread Pareto optimal solutions.

Second, when $\widehat{\mathcal{P}}_{\mathbf{y}} \not\leq \mathbf{R}$, mEI is equivalent to EHI but it is much easier to compute. Contrarily to EHI, mEI does not imply the computation of an m -dimensional hypervolume which potentially requires Monte-Carlo simulations (cf. Section 2.2). Its formula is analytical (substitute Equation (3) into (7)) and can easily be parallelized.

Proposition 4 (EHI-mEI equivalence). Let $Y_1(\cdot), \dots, Y_m(\cdot)$ be independent GPs fitted to the observations (\mathbb{X}, \mathbb{Y}) , with the associated empirical Pareto front $\widehat{\mathcal{P}}_{\mathbf{y}}$. If $\widehat{\mathcal{P}}_{\mathbf{y}} \not\leq \mathbf{R}$, $\text{EHI}(\cdot; \mathbf{R}) = \text{mEI}(\cdot; \mathbf{R})$.

Proof. Let $\widehat{\mathcal{P}}_{\mathbf{y}} \not\leq \mathbf{R}$. For such a reference point, the Hypervolume Improvement is

$$I_H(\mathbf{y}; \mathbf{R}) = H(\widehat{\mathcal{P}}_{\mathbf{y}} \cup \{\mathbf{y}\}; \mathbf{R}) - H(\widehat{\mathcal{P}}_{\mathbf{y}}; \mathbf{R}) = H(\{\mathbf{y}\}; \mathbf{R}) = \begin{cases} \prod_{j=1}^m (R_j - y_j) & \text{if } \mathbf{y} \preceq \mathbf{R} \\ 0 & \text{else} \end{cases}$$

With the $(\cdot)_+$ notation, $I_H(\mathbf{y}; \mathbf{R}) = \prod_{j=1}^m (R_j - y_j)_+$ and $\text{EHI}(\mathbf{x}; \mathbf{R})$ reduces to $\mathbb{E}[\prod_{j=1}^m (R_j - Y_j(\mathbf{x}))_+] = \prod_{j=1}^m \mathbb{E}[(R_j - Y_j(\mathbf{x}))_+]$ as the $Y_j(\cdot)$ are independent. This is the product of m Expected Improvements with objectives at the thresholds R_j . \square

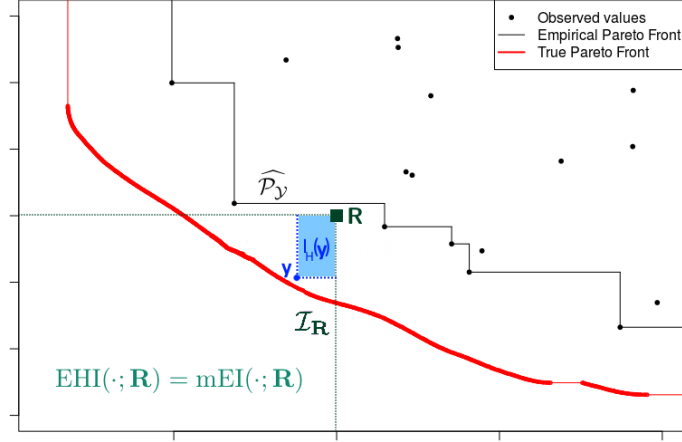


Figure 12: When using a non-dominated reference point w.r.t. $\widehat{\mathcal{P}}_{\mathcal{Y}}$, EHI and mEI are equivalent. The area in blue corresponds to a sample of both the product of improvements w.r.t. R_j and the Hypervolume Improvement.

Third, being a product of Expected Improvements, $\nabla \text{mEI}(\mathbf{x}; \mathbf{R})$ is computable as

$$\nabla \text{mEI}(\mathbf{x}; \mathbf{R}) = \sum_{i=1}^m \left[\nabla \text{EI}_i(\mathbf{x}; R_i) \prod_{\substack{j=1 \\ j \neq i}}^m \text{EI}_j(\mathbf{x}; R_j) \right]$$

where $\nabla \text{EI}(\mathbf{x}; \mathbf{R})$ has closed form, see [44] for instance. This offers the additional possibility of combining global optimization with gradient based methods when maximizing $\text{mEI}(\cdot; \mathbf{R})$. In comparison, EHI's gradient has no closed-form.

As we shall soon observe with the numerical experiments in Section 7, mEI is an efficient infill criterion for attaining the Pareto front provided that \mathbf{R} is taken in the non-dominated neighborhood of the Pareto front. It is important that \mathbf{R} is not dominated, not only for the equivalence with EHI to hold. Indeed, mEI with a dominated \mathbf{R} may lead to clustering: let $\mathbf{y}^{i_0} = \mathbf{f}(\mathbf{x}^{i_0}) \in \mathcal{P}_{\mathcal{Y}}$ such that $\mathbf{y}^{i_0} \preceq \mathbf{R}$. Then, because improvement over \mathbf{R} is certain at \mathbf{x}^{i_0} , $\text{mEI}(\mathbf{x}^{i_0}; \mathbf{R})$ will be large and often maximal in the vicinity of \mathbf{x}^{i_0} . Clustering in both the objective and the design space will be a consequence, leading to ill-conditioned covariance matrices. Taking a non-dominated reference point instead will diminish this risk as $\prod_{j=1}^m (R_j - y_j)_+ = 0 \quad \forall \mathbf{y} \in \widehat{\mathcal{P}}_{\mathcal{Y}}$, and no already observed solution will attract the search. If the reference point is too optimistic, the mEI criterion makes the search exploratory as the only points \mathbf{x} where progress is achieved during GP sampling are those with a large associated uncertainty $s^2(\mathbf{x})$. A clear example of a too optimistic reference point comes from the straightforward generalization of the default single objective $\text{EI}(\cdot; f_{\min})$ to multiple objectives: it is the criterion $\prod_{j=1}^m \text{EI}(\cdot; f_{j, \min}) \equiv \text{mEI}(\cdot; \mathbf{I})$, that is, the mEI criterion with the

empirical Ideal as the reference point (Figure 13). In non-degenerated problems where the Ideal is unattainable, sequentially maximizing $\text{mEI}(\cdot; \mathbf{I})$ will be close to sequentially maximizing $s^2(\mathbf{x})$.

Thus, \mathbf{R} has to be set up adequately. This is achieved in the proposed C-EHI algorithm by selecting the estimated Pareto front center as reference point and maximizing $\text{mEI}(\mathbf{x}; \hat{\mathbf{C}})$.

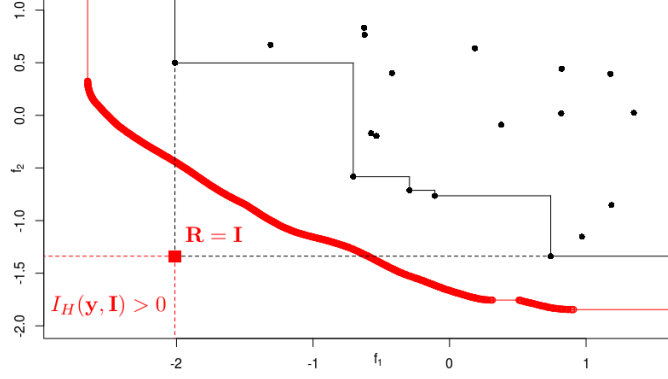


Figure 13: The product of Expected Improvements w.r.t. each minimum is equivalent to $\text{EHI}(\cdot; \mathbf{I})$. Only \mathbf{y} 's located in the bottom left corner would contribute to the Hypervolume Improvement. As such \mathbf{y} 's are both unattainable and located far away from the current front, maximizing $\text{EHI}(\cdot; \mathbf{I})$ will lead to exploration (i.e., lead to designs with largest uncertainty), hence an unsatisfactory optimization technique.

5 Detecting local convergence to the Pareto front

The Pareto front center may be reached before depletion of the computational resources. If the algorithm continues targeting the same region, it can no longer improve the center, and the infill criterion will favor the most uncertain parts of the design space. It is necessary to detect convergence to the center so that a broader part of the Pareto front can be searched in the remaining iterations, as will be explained in Section 6. In this section, we propose a novel method for checking convergence to the center. It does not utilize the mEI value which was found too unstable to yield a reliable stopping criterion: mEI is not normalized and heavily depends on the chosen reference point, which changes at each iteration. It may lead to premature stopping as shown in Figure 14.

Instead, the devised test relies on a measure of local uncertainty.

To test the convergence to a local part of the Pareto front, we define the *probability of domination in the Y space*³, $p(\mathbf{y})$, as the probability that there exists $\mathbf{y}' \in Y : \mathbf{y}' \preceq \mathbf{y}$. \mathbf{y} 's for which $p(\mathbf{y})$ is close to 0 or to 1 have a small or large probability, respectively, that there exist objective vectors dominating them. On the contrary, $p(\mathbf{y})$ close to 0.5 indicates no clear knowledge about the chances to find better vectors than \mathbf{y} . $p(\mathbf{y})$ measures how certain domination or non-domination of \mathbf{y} is. Formally, the domination $d(\mathbf{y})$ is a binary variable that equals 1 if $\exists \mathbf{x} \in X : \mathbf{f}(\mathbf{x}) \preceq \mathbf{y}$ and 0 otherwise. The Pareto front being a boundary for domination, d can also be expressed in the

³The probability of domination is also called “attainment function” in [9].

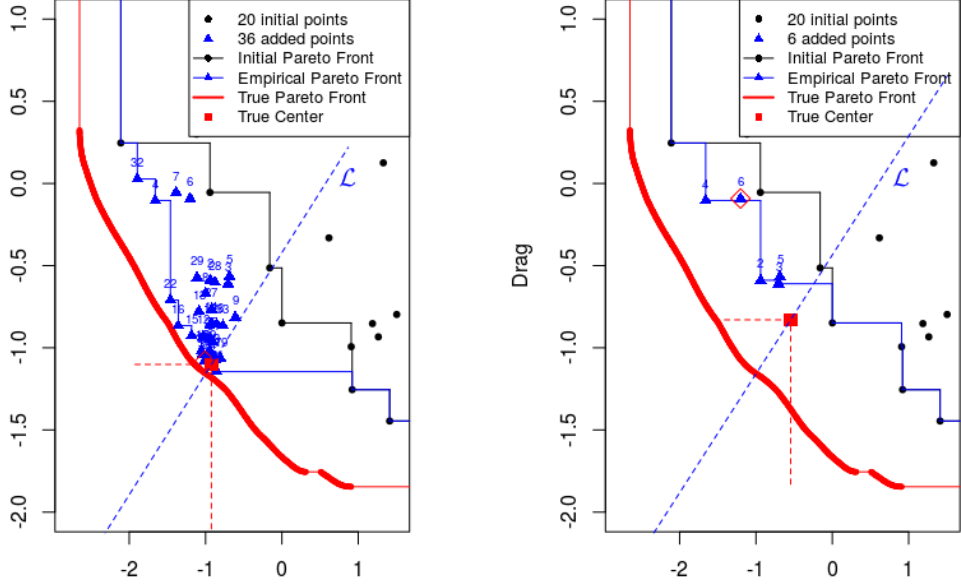


Figure 14: Pareto front approximation at local convergence detection. Our stopping criterion (left), based on the uncertainty along \mathcal{L} triggers after 36 iterations. The center of $\mathcal{P}_{\mathbf{y}}$ has clearly been attained. Even with a very small threshold ($\varepsilon = 5 \times 10^{-4}$ here), considering the value of mEI as a stopping criterion (right), has led to premature convergence (6 iterations, $\text{mEI}(\mathbf{x}^{(n+6)}; \mathbf{R}) = 2.4 \times 10^{-4}$ but convergence to \mathbf{C} has not occurred).

following way

$$d(\mathbf{y}) = \begin{cases} 1 & \text{if } \mathcal{P}_{\mathbf{y}} \preceq \mathbf{y} \\ 0 & \text{otherwise} \end{cases}$$

$d(\mathbf{y})$ can be seen as a binary classifier between dominated and non-dominated vectors whose frontier is the Pareto front and which is only known for previous observations $\mathbf{y} \in \mathbb{Y}$. We now consider an estimator $D(\mathbf{y})$ of $d(\mathbf{y})$ that has value 1 when the random Pareto front of the GPs, $\mathcal{P}_{\mathbf{Y}(\cdot)}$, dominates \mathbf{y} , and has value 0 otherwise,

$$D(\mathbf{y}) = \mathbb{1}(\mathcal{P}_{\mathbf{Y}(\cdot)} \preceq \mathbf{y})$$

The reader interested in theoretical background about the random set $\mathcal{P}_{\mathbf{Y}(\cdot)}$ is referred to [38, 9]. $D(\mathbf{y})$ is a Bernoulli variable closely related to the domination probability through $p(\mathbf{y}) = \mathbb{P}(D(\mathbf{y}) = 1) = \mathbb{E}[D(\mathbf{y})]$. If $p(\mathbf{y})$ goes quickly from 0 to 1 as \mathbf{y} crosses the Pareto front, the front is precisely known around this \mathbf{y} .

Making use of the probabilistic nature of the surrogate, and the independence between the m GPs, the probability that the image of a given input \mathbf{x} (through the surrogate) dominates \mathbf{y} is computable in closed-form $\forall \mathbf{x} \in X$: $\mathbb{P}(\mathbf{Y}(\mathbf{x}) \preceq \mathbf{y}) = \prod_{j=1}^m \Phi\left(\frac{y_j - \hat{y}_j(\mathbf{x})}{s_j(\mathbf{x})}\right)$

Remark 2. $\mathbb{P}(\mathbf{Y}(\mathbf{x}) \preceq \mathbf{y})$ can be regarded as an infill criterion in the decision space: given a target vector \mathbf{y} (e.g. the center of the Pareto front), this infill criterion will select the point in X space

having the greatest probability of dominating \mathbf{y} . This infill criterion can be viewed as a multi-objective extension to the mono-objective Probability of Improvement [28]. It however did not show as large benefits as mEI as it does not reward the magnitude of domination, and encourages small but non-risky improvements over \mathbf{y} .

As the $Y_j(\cdot)$ are independent, it is easy to calculate the probability of domination for a specific \mathbf{x} , $\mathbb{P}(\mathbf{Y}(\mathbf{x}) \preceq \mathbf{y}) = \prod_{j=1}^m \Phi\left(\frac{y_j - \hat{y}_j(\mathbf{x})}{s_j(\mathbf{x})}\right)$. In contrast, the probability of dominating \mathbf{y} at any \mathbf{x} by $\mathbf{Y}(\mathbf{x})$, $\mathbb{P}(\exists \mathbf{x} \in X : \mathbf{Y}(\mathbf{x}) \preceq \mathbf{y})$, has no closed-form as many overlapping cases occur. Even for a discrete set $\mathbb{S} = \{\mathbf{x}^{n+1}, \dots, \mathbf{x}^{n+s}\}$, $\mathbb{P}(\exists \mathbf{x} \in \mathbb{S} : \mathbf{Y}(\mathbf{x}) \preceq \mathbf{y})$ has to be estimated by numerical simulation because of the correlations in the Gaussian vector $\mathbf{Y}(\mathbb{S})$, as the latter rewrites $1 - \mathbb{P}(\mathbf{Y}(\mathbf{x}^{n+1}) \not\preceq \mathbf{y}, \dots, \mathbf{Y}(\mathbf{x}^{n+s}) \not\preceq \mathbf{y})$ which has also no closed form because of both the correlations in the Gaussian vector $\mathbf{Y}(\mathbb{S})$ ($\mathbb{P}(\mathbf{Y}(\mathbf{x}^{n+1}) \not\preceq \mathbf{y}, \dots, \mathbf{Y}(\mathbf{x}^{n+s}) \not\preceq \mathbf{y}) \neq \prod_{i=1}^s \mathbb{P}(\mathbf{Y}(\mathbf{x}^{n+i}) \not\preceq \mathbf{y})$) and the overlapping of non-dominated subspaces.

Alternatively, replacing $p(\mathbf{y})$ by its lower bound $\mathbb{P}(\exists \mathbf{x} \in X : \mathbf{Y}(\mathbf{x}) \preceq \mathbf{y}) \geq \max_{\mathbf{x} \in X} \mathbb{P}(\mathbf{Y}(\mathbf{x}) \preceq \mathbf{y})$ could be a substitute with a high computational complexity since it involves solving an optimization problem in d variables each time $p(\mathbf{y})$ is needed.

To estimate the probability $p(\mathbf{y})$ that an objective vector \mathbf{y} can be dominated, we exploit the probabilistic nature of the GPs conditioned by previous observations: we simulate n_{sim} GPs, from which we extract the corresponding Pareto fronts $\widetilde{\mathcal{P}}_{\mathbf{y}}^{(k)}$, $k = 1, \dots, n_{sim}$. $D^{(k)}$ is a realization of the estimator and random variable $D(\mathbf{y})$,

$$D^{(k)}(\mathbf{y}) = \mathbb{1}(\widetilde{\mathcal{P}}_{\mathbf{y}}^{(k)} \preceq \mathbf{y}) = \begin{cases} 1 & \text{if } \exists \mathbf{z} \in \widetilde{\mathcal{P}}_{\mathbf{y}}^{(k)} : \mathbf{z} \preceq \mathbf{y} \\ 0 & \text{otherwise} \end{cases}$$

Therefore, $p(\mathbf{y})$ which is the mean of $D(\mathbf{y})$ can be estimated by averaging the realizations,

$$p(\mathbf{y}) = \lim_{n_{sim} \rightarrow \infty} \widehat{p}(\mathbf{y}) \quad \text{where} \quad \widehat{p}(\mathbf{y}) = \frac{1}{n_{sim}} \sum_{k=1}^{n_{sim}} D^{(k)}(\mathbf{y}).$$

One can easily check that $\widehat{p}(\mathbf{y})$ is monotonic with domination: if $\mathbf{y}' \preceq \mathbf{y}$, then every $\widetilde{\mathcal{P}}_{\mathbf{y}}^{(k)}$ dominating \mathbf{y}' will also dominate \mathbf{y} and $\widehat{p}(\mathbf{y}') \leq \widehat{p}(\mathbf{y})$.

As discussed in Section 3.3, the choice of points $\mathbf{x}^{n+i} \in X$, $i = 1, \dots, s$ where the GP simulations are performed is crucial. Here, as the simulated Pareto fronts aim at being possible versions of the true front, the \mathbf{x} 's are chosen according to their probability of being non-dominated with regard to the current approximation $\widetilde{\mathcal{P}}_{\mathbf{y}}$ in a roulette wheel selection procedure [14] to maintain both diversity and a selection pressure. Using a space-filling DoE [47, 24, 39] for the simulations would lead to less dominating simulated fronts, and to an under-estimated probability of dominating \mathbf{y} . Another advantage of this technique is that the computational burden resides in the \mathbf{x} selection procedure and the simulation of the GPs. Once the simulated fronts have been generated, $p(\cdot)$ can be estimated for many \mathbf{y} 's $\in Y$ without significant additional effort.

The variance of the Bernoulli variable $D(\mathbf{y})$ is $p(\mathbf{y})(1 - p(\mathbf{y}))$ and can be interpreted as a measure of uncertainty about dominating \mathbf{y} . When $p(\mathbf{y}) = 1$ or 0, no doubt subsists regarding the fact that \mathbf{y} is dominated or non-dominated, respectively. When half of the simulated fronts dominate \mathbf{y} , $p(\mathbf{y}) = 0.5$ and $p(\mathbf{y})(1 - p(\mathbf{y}))$ is maximal: uncertainty about the domination of \mathbf{y} is at its highest.

Here, we want to check convergence to the Pareto front center which, by definition, is located on the estimated Ideal-Nadir line $\widehat{\mathcal{L}}$. We therefore consider the uncertainty measure $(p(\mathbf{y})(1 - p(\mathbf{y})))$

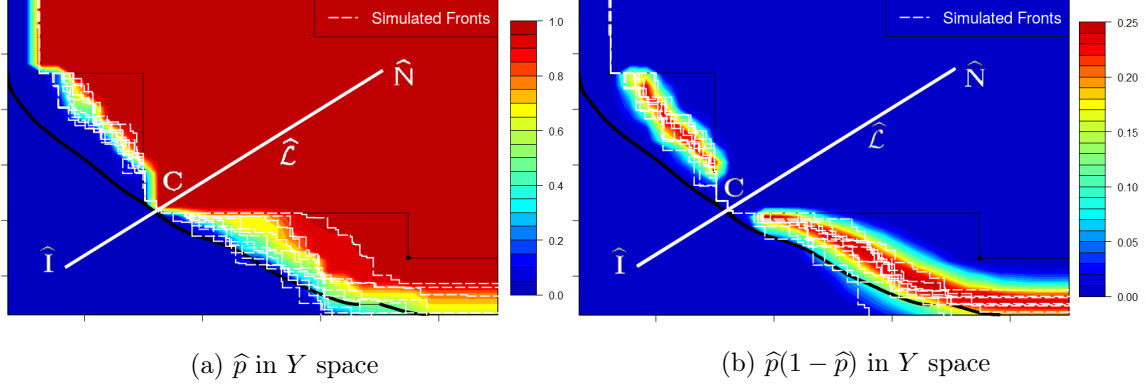


Figure 15: Detection of convergence to the Pareto front center using simulated fronts. Five of the $n_{sim} = 200$ simulated fronts are shown. The approximation $\widehat{\mathcal{P}}_Y$ (thin black line) has converged towards \mathcal{P}_Y (thick black curve) at the center of the front (intersection with $\widehat{\mathcal{L}}$). Consequently, $p(\mathbf{y})$ grows very fast from 0 to 1 along $\widehat{\mathcal{L}}$ and the domination uncertainty on the right plot $p(\mathbf{y})(1 - p(\mathbf{y}))$ is null.

for \mathbf{y} varying along $\widehat{\mathcal{L}}$, convergence at the center being equivalent to a sufficiently small uncertainty of $D(\mathbf{y})$ along $\widehat{\mathcal{L}}$. This leads to saying that convergence to the center has occurred if the *line uncertainty* is below a threshold, $U(\widehat{\mathcal{L}}) < \varepsilon$, where the line uncertainty is defined as

$$U(\widehat{\mathcal{L}}) := \frac{1}{|\widehat{\mathcal{L}}|} \int_{\widehat{\mathcal{L}}} p(\mathbf{y})(1 - p(\mathbf{y})) d\mathbf{y} . \quad (8)$$

$|\widehat{\mathcal{L}}|$ is the (Euclidean) distance between the estimated Ideal and Nadir points and ε is a small positive threshold. Figure 15 illustrates a case of detection of convergence to the Pareto front center. On the left plot, when moving along $\widehat{\mathcal{L}}$ from $\widehat{\mathbf{I}}$ to $\widehat{\mathbf{N}}$, $p(\cdot)$ goes quickly from 0 to 1 when crossing the estimated and real Pareto fronts. The variability between the simulated Pareto fronts is low in the central part, as seen on the right plot: $p(\mathbf{y})(1 - p(\mathbf{y}))$ equals 0 (up to estimation precision) all along $\widehat{\mathcal{L}}$ and in particular near the center of the approximation front where sufficiently many points $\mathbf{f}(\mathbf{x})$ have been observed and no further improvement can be achieved.

If $p(\mathbf{y})$ equals either 0 or 1 along $\widehat{\mathcal{L}}$, all n_{sim} simulated fronts are intersected at the same location by $\widehat{\mathcal{L}}$, thus convergence is assumed in this area. To set the threshold ε , we consider that convergence has occurred in the following limit scenarios: as there are 100 integration points on $\widehat{\mathcal{L}}$ for the computation of the criterion (8), $p(\mathbf{y})$ jumps successively from 0 to 0.01 and 1 (or from 0 to 0.99 and 1); or $p(\mathbf{y})$ jumps successively from 0 to 0.005, 0.995 and 1. This rule leads to a threshold $\varepsilon = 10^{-4}$. This threshold is implicitly depending on the number of simulated fronts n_{sim} we use. Indeed, $p(\mathbf{y}) \leq 0.005$ means less than 0.5% of the simulated fronts dominate \mathbf{y} .

6 Expansion of the approximation front within the remaining budget

If convergence to the center of the Pareto front is detected and the objective functions budget is not exhausted, the goal is no longer to search at the center where no direct progress is possible, but to investigate a *wider central part* of the Pareto front. A second phase of the algorithm is started during which a new, fixed, reference point \mathbf{R} is set for the EHI infill criterion. To continue targeting the central part of the Pareto front, the new \mathbf{R} has to be located on $\hat{\mathcal{L}}$. The more distant \mathbf{R} is from \mathcal{P}_Y , the broader the targeted area in the objective space will be, as $\mathcal{I}_{\mathbf{R}} \subset \mathcal{I}_{\mathbf{R}'}$ if $\mathbf{R} \preceq \mathbf{R}'$. As shown in Figure 16, \mathbf{R} is instrumental in deciding in which area solutions are sought. After having spent the b remaining calls to the objective functions, we would like to have (i) an approximation front $\widehat{\mathcal{P}}_Y$ as broad as possible, (ii) which has converged to \mathcal{P}_Y in the entire targeted area $\mathcal{I}_{\mathbf{R}}$. These goals are conflicting: at a fixed budget b , the larger the targeted area, the least \mathcal{P}_Y will be well described. The reference point leading to the best trade-off between convergence to the Pareto front and width of the final approximation front is sought.

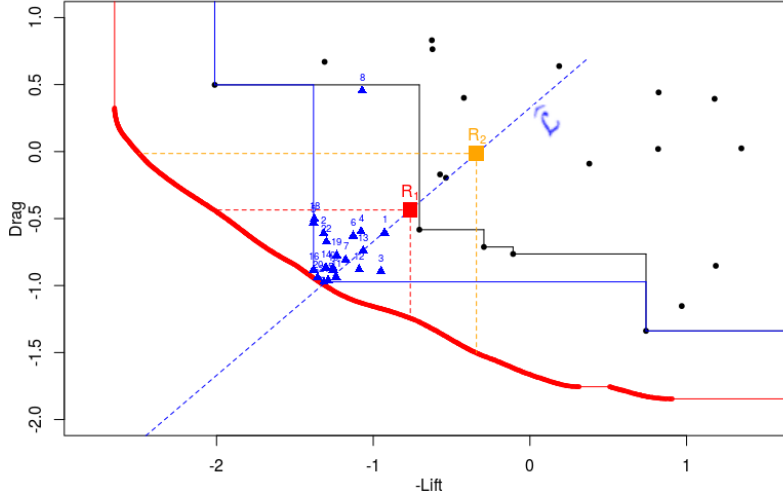


Figure 16: Two possible reference points \mathbf{R}_1 and \mathbf{R}_2 located on $\hat{\mathcal{L}}$, and the part of the Pareto front they allow to target when used within EHI

6.1 Anticipating the final approximation front via virtual infills

To choose the *best* reference point for the remaining b iterations, we anticipate the behavior of the algorithm and the final approximation front obtained with a given \mathbf{R} . Candidate reference points $\mathbf{R}^c, c = 1, \dots, C$, are uniformly distributed along $\hat{\mathcal{L}}$ with $\mathbf{R}^0 = \hat{\mathbf{C}}$ and $\mathbf{R}^C = \hat{\mathbf{N}}$. Each \mathbf{R}^c is related to an area in the objective space it targets, $\mathcal{I}_{\mathbf{R}^c}$. Starting from the current GPs $\mathbf{Y}(\cdot)$, C virtual optimization scenarios are anticipated by sequentially maximizing EHI b times for each candidate reference point \mathbf{R}^c . We use a Kriging Believer [23] strategy in which the metamodel is augmented at each virtual iteration using the kriging mean $\hat{\mathbf{y}}(\mathbf{x}^{*i})$, \mathbf{x}^{*i} being the maximizer of $\text{EHI}(\cdot; \mathbf{R}^c)$ at

one of the virtual step $i \in \{1, \dots, b\}$. Such a procedure does not modify the posterior mean $\hat{\mathbf{y}}(\cdot)$, but it changes the posterior variance $\mathbf{s}^2(\cdot)$. The conditional GPs $\mathbf{Y}(\cdot)$ *augmented* by these b Kriging Believer steps are denoted as $\mathbf{Y}^{KB}(\cdot)$. The accuracy of the GPs is variable in the different parts of the Pareto front (typically high in the central part of $\mathcal{P}_{\mathcal{Y}}$, whereas it may be poor in regions of $\mathcal{P}_{\mathcal{Y}}$ that have been less explored). Thus, taking the uncertainty of the metamodel into account, e.g. using draws from the posterior instead of the kriging mean for the virtual infills has also been considered, the drawback being an additional cost: several draws would be required, augmenting the amount of virtual fronts to analyze.

The optimizations for the \mathbf{R}^c 's are independent and parallel computing can be exploited (in our implementation, it has been done through the `foreach R` package). At the end, C different final Kriging Believer GPs $\mathbf{Y}^{KB}(\cdot)$ are obtained that characterize the associated \mathbf{R}^c . \mathbf{R} 's close to the center produce narrow and densely sampled final fronts whereas distant \mathbf{R} 's lead to more extended and sparsely populated fronts, as can be seen in Figure 17.

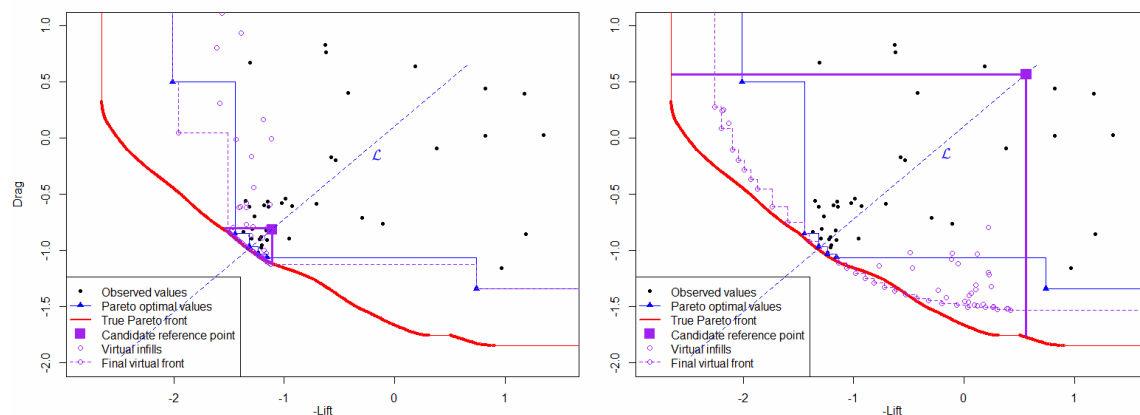


Figure 17: Virtual infills obtained by sequentially maximizing $\text{EHI}(\cdot; \mathbf{R})$ b times, for two different reference points (purple squares). The shape and sampling density of the final virtual front depends on \mathbf{R} .

6.2 Virtual front uncertainty for determining the targeted area

To measure how much is known about the Pareto front, we generalize the line uncertainty of Equation (8) to the volume $\mathcal{I}_{\mathbf{R}}$ and define the *volume uncertainty*, $U(\mathbf{R}; \mathbf{Y})$ of the GPs $\mathbf{Y}(\cdot)$. The volume uncertainty is the average domination uncertainty $p(\mathbf{y})(1 - p(\mathbf{y}))$ in the volume that dominates \mathbf{R} bounded by the Ideal point where $p(\mathbf{y})$ is calculated for $\mathbf{Y}(\cdot)$,

$$U(\mathbf{R}; \mathbf{Y}) := \frac{1}{\text{Vol}(\mathbf{I}, \mathbf{R})} \int_{\mathbf{I} \leq \mathbf{y} \leq \mathbf{R}} p(\mathbf{y})(1 - p(\mathbf{y})) d\mathbf{y} . \quad (9)$$

In practice, the estimated Ideal $\hat{\mathbf{I}}$ is substituted for the Ideal. $U(\mathbf{R}; \mathbf{Y})$ quantifies the *convergence* to the estimated Pareto front in the progress region delimited by \mathbf{R} . It is a more rigorous uncertainty measure than others based on the density of points in the \mathcal{Y} space as it accounts for the possibility of having many inverse images \mathbf{x} to \mathbf{y} .

The optimal reference point is the one that creates the largest and sufficiently well populated Pareto front. The concepts of augmented GPs and volume uncertainty to measure convergence allow to define the *optimal reference point*,

$$\mathbf{R}^* := \mathbf{R}^{c^*} \quad \text{where} \quad c^* = \max_{c=1,\dots,C} c \quad (10)$$

such that $U(\mathbf{R}^c; \mathbf{Y}^{KB}) < \varepsilon$

Note that the uncertainty is calculated with the augmented GPs $\mathbf{Y}^{KB}(\cdot)$, i.e., the domination probabilities $p(\mathbf{y})$ in Equation (9) are obtained with $\mathbf{Y}^{KB}(\cdot)$. Associated to \mathbf{R}^* is the *optimal improvement region*, $\mathcal{I}_{\mathbf{R}^*}$, that will be the focus of the search in the second phase. For \mathbf{R}^* to be able to depart from the center, a threshold ε 10 times larger as the one of Equation (8) is applied. The procedure for selecting \mathbf{R} after local convergence is illustrated in Figures 18 and 19. The initial DoE is made of 20 points and $\varepsilon = 10^{-3}$. Convergence to the center is detected after 26 added points, leaving $b = 54$ points in the second phase of the algorithm for a total budget of 100 $\mathbf{f}(\cdot)$ evaluations. Figure 18 shows the final virtual Pareto fronts obtained for two different reference points, as well as simulated fronts sampled from the final virtual posterior (those fronts are used for measuring the uncertainty). On the left, the area targeted by \mathbf{R} is small, and so is the remaining uncertainty ($U(\mathbf{R}; \mathbf{Y}^{KB}) = 3 \times 10^{-6} < 10^{-3}$). On the right, a farther \mathbf{R} leads to a broader approximation front, but to higher uncertainty ($U(\mathbf{R}; \mathbf{Y}^{KB}) = 0.0015 > 10^{-3}$). Figure 19 represents the approximation front obtained when using the optimal \mathbf{R}^* ($U(\mathbf{R}^*; \mathbf{Y}^{KB}) = 9.4 \times 10^{-4}$) of Equation (10). A complete covering of $\mathcal{P}_{\mathcal{Y}}$ in the targeted area is observed. As the remaining budget after local convergence was important in this example (54 iterations), the Pareto front has been almost entirely unveiled. In the case of smaller remaining budgets, larger Pareto fronts or greater number of objectives, the chosen reference point would target a smaller part of $\mathcal{P}_{\mathcal{Y}}$.

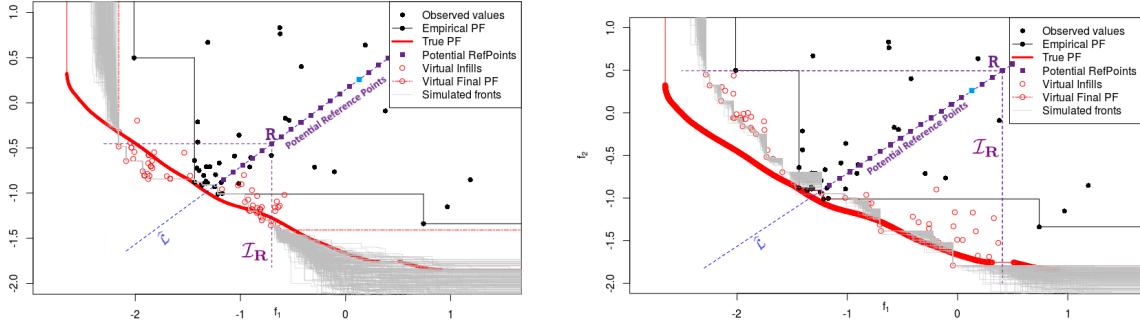


Figure 18: Uncertainty quantification through final virtual fronts. The anticipated remaining uncertainty can be visualized as the grey area within \mathcal{I}_R roamed by the sampled fronts. It is small enough for the \mathbf{R} used on the left and too important for the \mathbf{R} on the right. The blue reference point on $\hat{\mathcal{L}}$ is \mathbf{R}^* , the farthest point that leads to a virtual front with low enough uncertainty.

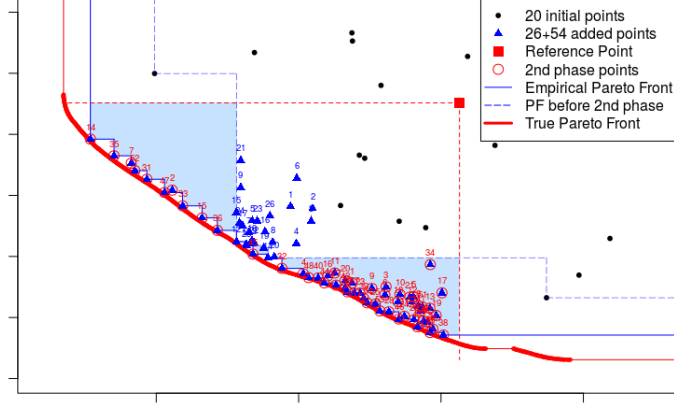


Figure 19: Final approximation of the Pareto front with, as a red square, the reference point of the second phase chosen as a solution to Problem (10), $\mathbf{R} = \mathbf{R}^*$. The objectives values added during the second phase of the algorithm are circled in red. Compared to the initial front obtained when searching for the center, the last approximation front is expanded as highlighted by the blue hypervolume.

7 Algorithm implementation and testing

7.1 Implementation of the C-EHI algorithm

The concepts and methods defined in Sections 3 to 6 are put together to make the C-EHI algorithm which stands for Centered Expected Hypervolume Improvement. The R package `DiceKriging` has been used for building the Gaussian processes and additional implementations were written in the R language. The C-EHI algorithm was sketched in Figure 1 and is further detailed in Algorithm 1. The integral for $U(\hat{\mathcal{L}})$ is estimated numerically using $N = 100$ points regularly distributed along $\hat{\mathcal{L}}$. $U(\mathbf{R})$ is computed by means of Monte-Carlo techniques with $N = 10^5$ samples.

7.2 Meta NACA: a practical performance test bed

Comparing the efficiency of multi-objective optimizers is a difficult task because the performance of the algorithms depends on the test functions and a proper metric needs to be chosen to compare the Pareto fronts. The COCO platform [11] allows the comparison of bi-objective optimizers on a general set of functions with the hypervolume improvement (calculated with respect to the Nadir point) as a performance measure. In the spirit of MOPTA [29], the choice was made here to test the optimizers on a set of functions that were designed to represent the real-world problems of interest.

The test set is called Meta NACA. It has been built by combining surrogate modeling techniques and aerodynamic data coming from 2D simulations of the flow around a NACA airfoil. More precisely, for each aerodynamic objective, a GP with a Matérn 5/2 kernel is first fit to an initial large space-filling DoE of 1000 designs. The evaluation of the aerodynamic performance of one design has a cost of approximately 15 minutes (wall clock time, on a standard personal computer). Exploiting parallel computation, the evaluation of such a large DoE remains affordable. Next, a sequential Bayesian multi-objective optimization infill criterion (as described in Section 2) is

Algorithm 1 C-EHI (Centered Expected Hypervolume Improvement)

Inputs: uncertainty limit ε , *budget*

```
create an initial DoE of  $n$  points;
initialize  $m$  GPs for each objective  $f_i, i = 1, \dots, m$ ; # see Section 2.1
 $t = n$ ;  $U(\hat{\mathcal{L}}) = +\infty$ ; #  $U(\hat{\mathcal{L}})$  line uncertainty, Eq. (8)
# First phase: optimization towards the center
while ( $U(\hat{\mathcal{L}}) > \varepsilon$ ) and ( $t \leq \text{budget}$ ) do
    estimate  $\hat{\mathbf{I}}, \hat{\mathbf{N}}$  and  $\hat{\mathbf{C}}$ ; # see Section 3
     $\mathbf{x}^{(t+1)} = \arg \max_{\mathbf{x} \in X} \text{mEI}(\mathbf{x}; \hat{\mathbf{C}})$ ; # see Section 4
    evaluate  $\mathbf{f}(\mathbf{x}^{(t+1)})$  and update the GPs; # see Section 2.1
    compute  $U(\hat{\mathcal{L}})$ ; # see Section 5
     $t = t + 1$ ;
end while
# If remaining budget after convergence: second phase
# Determine widest accurately attainable area and target it, see Section 6
if  $t \leq \text{budget}$  then
    choose  $\mathbf{R}^*$  solution of Eq. (10); # see Section 6
     $\mathbf{R}^* = \arg \min_{\substack{\mathbf{R} \in \hat{\mathcal{L}} \\ U(\mathbf{R}; \mathbf{Y}^{KB}) < \varepsilon}} \|\mathbf{R} - \hat{\mathbf{N}}\|$ ;
end if
while  $t \leq \text{budget}$  do
     $\mathbf{x}^{(t+1)} = \arg \max_{\mathbf{x} \in X} \text{EHI}(\mathbf{x}; \mathbf{R}^*)$ ; # target larger improvement region  $\mathcal{I}_{\mathbf{R}^*}$ 
    evaluate  $f_i(\mathbf{x}^{(t+1)})$  and update the GPs;
     $t = t + 1$ ;
end while
return final DoE, final GPs, and approximation front  $\hat{\mathcal{P}}_{\mathbf{y}}$ 
```

employed to enrich the DoE. The goal of this step is to enhance the GPs in promising areas that are likely to be visited by a multi-objective optimizer. Last, 100 additional designs, drawn randomly in the design space are evaluated. While these last points will help in improving the accuracy, they are mainly useful in removing any artificial periodicity in the design space due to space-filling properties which might hinder the estimation of correlation parameters. The evaluation, that is to say the computation of the kriging mean of the final GPs is very rapid (less than 0.1s on a personal computer), and has turned out to be an accurate substitute to the aerodynamic simulations after validation (Q2 between 0.96 and 0.99). The whole process of approximation building by a GP was repeated for the variable dimensions (CAD parameters) $d = 3, 8, 22$ and $m = 2$ to 4 objectives (lift and drag at 2 different angles of attack). We also computed the “true” Pareto front by applying the NSGA-II MOO algorithm [16] to the kriging mean functions. In the following, experiments are only reported for $d = 8$ variables, which compromises the dimension of the problem and the time of one optimization run, but the same conclusions have been obtained for the cases $d = 3$ and $d = 22$. One typical run of the C-EHI algorithm for $d = 3$ and $d = 22$, $m = 2$ objectives is shown in Figures 20 and 21.

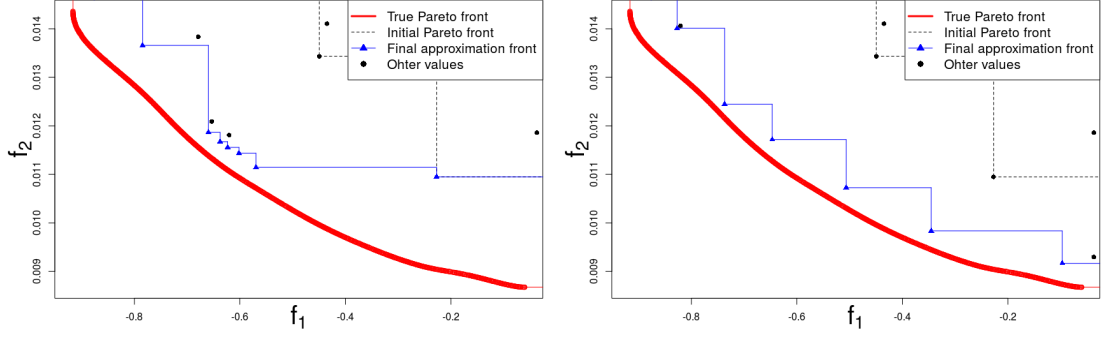


Figure 20: Comparison between C-EHI (left) and EHI (right) for one run of the Meta NACA problem in $d = 3$ dimensions. 20 calls to $\mathbf{f}(\cdot)$ were allowed and 10 of them were devoted to the initial DoE. C-EHI improves the Pareto front at its center, EHI tries to uncover the whole front at the cost of a lower accuracy.

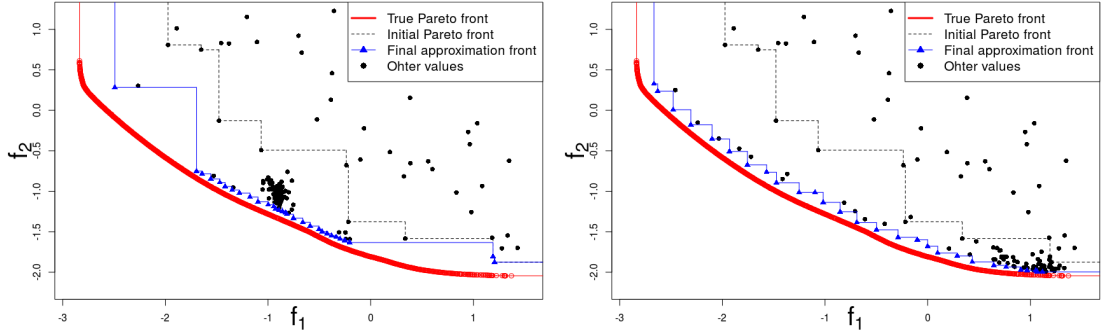


Figure 21: Comparison between C-EHI (left) and EHI (right) for one run of the Meta NACA problem in $d = 22$ dimensions. 150 calls to $\mathbf{f}(\cdot)$ were allowed and 50 of them were devoted to the initial DoE. Again, C-EHI improves the Pareto front at its center, EHI tries to uncover the whole front at the cost of a lower accuracy.

7.3 Performance metrics

To assess the behavior of the C-EHI algorithm, multi-objective performance metrics (see [34, 60] for some definitions and discussions) have to be employed. For comparing approximation fronts produced by an algorithm, considering several indicators is recommended [34]. In the following, we use three common metrics: the non-dominated Hypervolume [58] that we normalize with respect to the Hypervolume of the true Pareto front, and the Inverse Generational Distance (IGD) [12], which corresponds to the mean distance between points of a reference set (in our case the true Pareto front) and the approximation front. A modified version of the ε -Indicator [60] is also used for measuring the minimal distance to the Pareto front of an approximation front: $\varepsilon(\widehat{\mathcal{P}}_{\mathcal{Y}}; \mathcal{P}_{\mathcal{Y}}) := \min_{\mathbf{y} \in \widehat{\mathcal{P}}_{\mathcal{Y}}} \min \{ \varepsilon : \nexists \mathbf{z} \in \mathcal{P}_{\mathcal{Y}}, \mathbf{z} \preceq \mathbf{y} - \varepsilon \cdot \mathbf{1}_m \}$. It corresponds to the smallest value that has to be subtracted to $\widehat{\mathcal{P}}_{\mathcal{Y}}$ such that one of its solutions becomes non-dominated with regard to $\mathcal{P}_{\mathcal{Y}}$. To simplify, we will

refer to the ε -Indicator when considering this indicator. These metrics deal with approximations of the *whole* Pareto front, and empirical Pareto fronts having a similar shape to the one shown in blue in Fig. 16 will exhibit very bad performance, as they do not cover the entire front.

In order to focus on the central part of the Pareto front, the indicators are restricted to the regions of interest

$$\mathcal{I}_w := \{\mathbf{y} \in Y : \mathbf{y} \preceq \mathbf{R}^w\} \quad \text{where} \quad \mathbf{R}^w := (1 - w)\mathbf{C} + w\mathbf{N} .$$

To focus on the central part, $w = 0.1, 0.2$ or 0.3 . Figure 22 shows corresponding areas in Y space in the two-dimensional case. Notice that these truncated indicators will also show if our method was able to recover the real center of the Pareto front: if it was directed towards a wrong (in the sense not central) location of \mathcal{P}_Y during the first phase, the indicators will exhibit bad results. The ε -Indicator will also be considered with regard to the entire Pareto front, to show how close a solution from $\widehat{\mathcal{P}}_Y$ can be from \mathcal{P}_Y considered in its entirety. If C-EHI has detected convergence, the algorithm determines an “optimal improvement” region $\mathcal{I}_{\mathbf{R}^*}$ (defined in Section 6) where new values are sought during the last iterations. Indicator values in this part of the Pareto front are also of interest as this area is targeted within the last iterations.

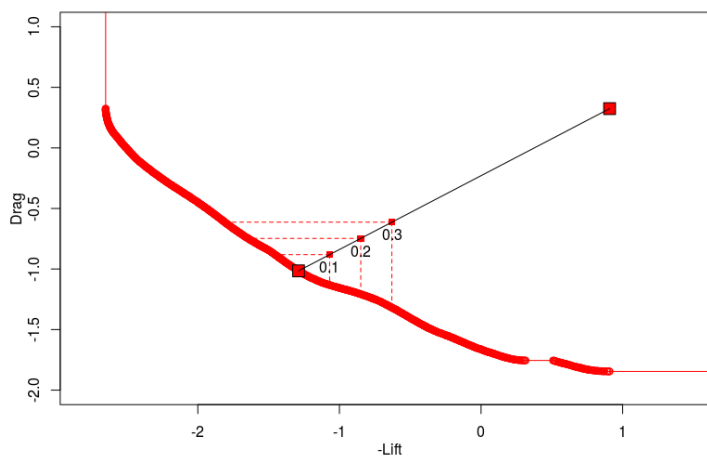


Figure 22: Central parts of the Pareto front for which the indicators are computed. The $\mathcal{I}_{0,1}$ area only considers extremely close and central solutions.

7.4 Test results

Figure 23 shows a typical run of our algorithm when facing a too restricted budget to uncover the Pareto front in its entirety. During the first iterations, the center of the Pareto front is targeted. Once local convergence has been detected, the part of the Pareto front in which convergence can be accurately obtained within the remaining budget is forecasted, and then targeted. The approximation of \mathcal{P}_Y has clearly been enhanced in its central part. The same results are observed with three or four objectives and a typical run with $m = 3$ is given in Figure 24. The targeting methodology gains in importance as the number of objectives increases because the relative number of Pareto optimal solutions grows and it becomes harder to approximate all of them.

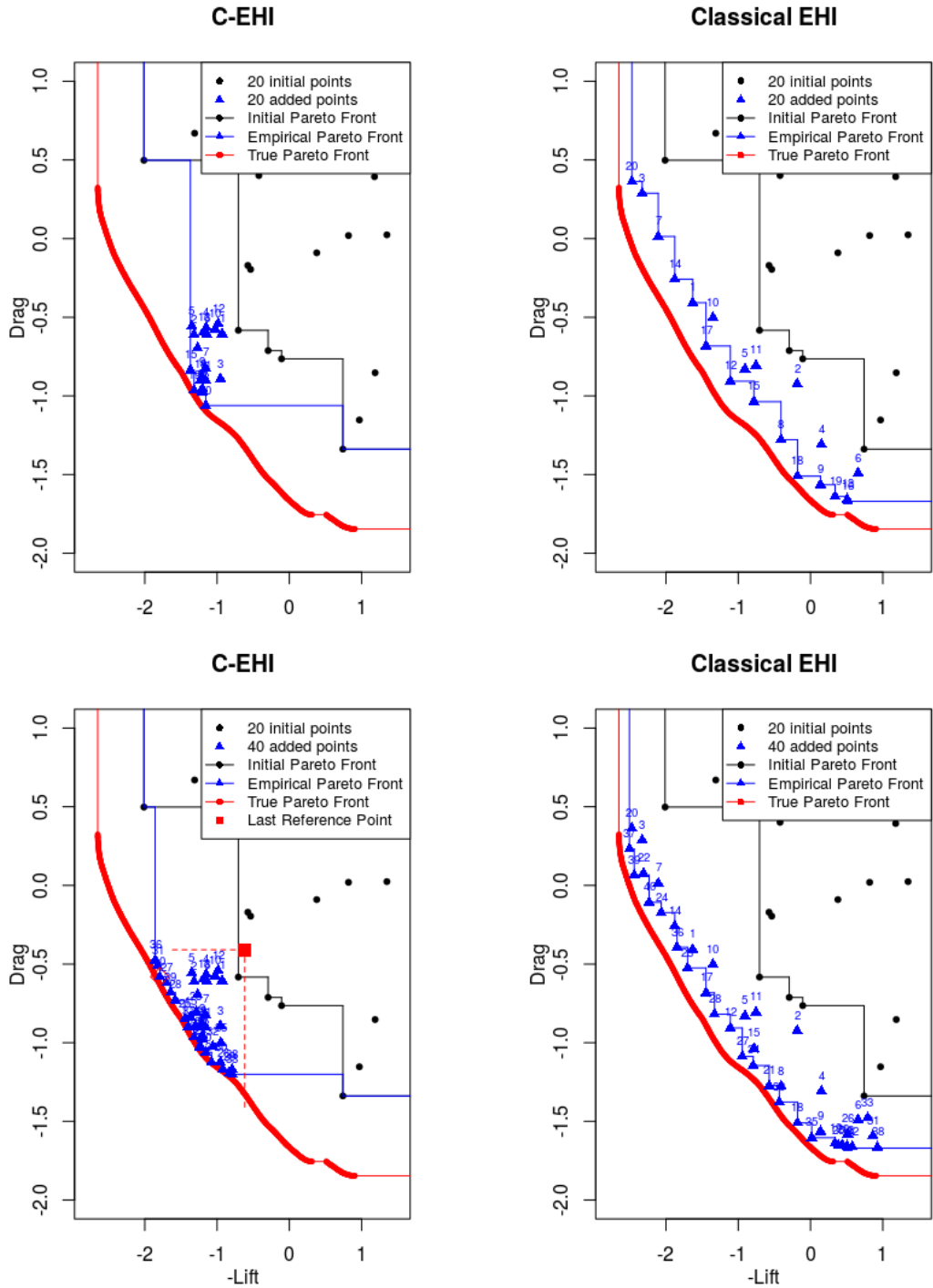


Figure 23: Comparison of C-EHI (left) with the standard EHI (right). Top: approximation front after 20 iterations: C-EHI better converges to the center of the Pareto front to the detriment of the front ends. Bottom: approximation front after 40 iterations: after local convergence (at the 22nd iteration here), a wider optimal improvement region (under the red square) is targeted for the 18 remaining iterations, is targeted by the algorithm. Compared to the standard EHI, the Pareto front is sought in a smaller balanced part of the objective space, at the advantage of a better convergence.

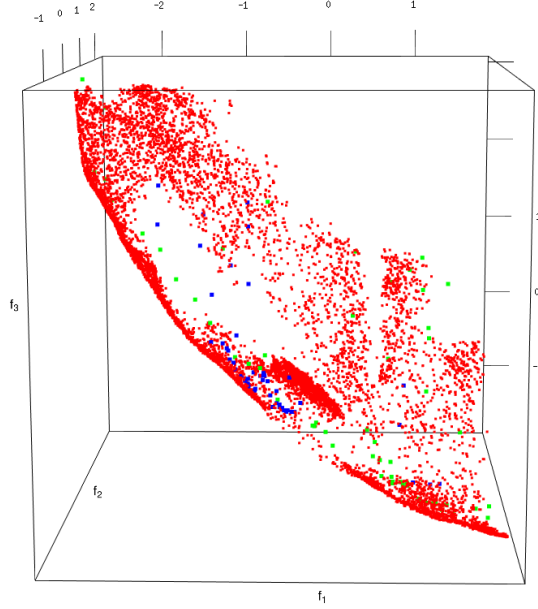


Figure 24: Typical C-EHI (blue points) and EHI (green points) runs on the Meta NACA problem with $m = 3$ objectives. The true Pareto front (red) is attained at its center by C-EHI while it is approximated globally yet less accurately by EHI.

The Tables below contain the Hypervolume Indicator, IGD, and modified ε -Indicator for 2, 3 and 4 objective test cases. They are computed in $\mathcal{I}_{0,1}$, $\mathcal{I}_{0,2}$ and $\mathcal{I}_{0,3}$, and averaged over 10 runs. Standard deviations are indicated in parentheses. The last column averages the indicator values restricted to $\mathcal{I}_{\mathbf{R}^*}$ over the runs that reached the second phase. A - indicates that no run has reached the second phase for the considered budget. Inf indicates that for at least one run, no solution was found in \mathcal{I}_w . The indicator values of the C-EHI algorithm are compared to those obtained with the standard EHI [20] implementation of the R package `GPareto` [8] (right column). In `GPareto`, the default reference point is taken at $\mathbf{N} + \mathbf{1}$. Dealing with extremely parsimonious uses of the computer code, 4 tight optimization budgets are considered: 40, 60, 80 and 100 calls to \mathbf{f} . The 20 first calls are devoted to the initialization of the GPs using an LHS space-filling design [48], and the experiments are repeated 10 times starting from different initial designs.

Figure 25 shows how the Hypervolume Indicator evolves with optimization iterations. The indicators are of course increasing with the iterations, and the C-EHI consistently outperforms the general EHI in finding points in the central part of the Pareto front for 2 and 3 objectives. For 4 objectives an important number of points obtained by both algorithms belongs to $\mathcal{I}_{0,2}$ and $\mathcal{I}_{0,3}$. While significantly more values (and Pareto-optimal values) are obtained by C-EHI in $\mathcal{I}_{0,2}$ and $\mathcal{I}_{0,3}$, the Hypervolume Indicator sometimes favours EHI.

A few words of caution are needed to read the Tables 1 to 3. As the width of the Pareto front that is targeted in the second phase depends on the remaining budget, runs of the C-EHI algorithm with different total budgets are not directly comparable. For instance, if convergence is detected after 35 iterations, the reference point that defines the targeted area for the last calculations \mathbf{R}^* will be different if 5 or 45 iterations remain. The first case will concentrate on a very central part of the

Pareto front, whereas the second will target a broader area. As a consequence, some numbers may express better performance in thinner portions of the Pareto front in spite of a smaller total budget, which is only due to the fact that they have explicitly targeted a smaller part of the solutions.

m	$budget$	$\mathbf{R}^{0.1}$		$\mathbf{R}^{0.2}$		$\mathbf{R}^{0.3}$		\mathbf{R}^*	
		C-EHI	EHI	C-EHI	EHI	C-EHI	EHI	C-EHI	EHI
2	40	0.275 (0.18)	0.025 (0.04)	0.498 (0.17)	0.227 (0.15)	0.581 (0.10)	0.386 (0.19)	0.664	0.253
	60	0.377 (0.19)	0.096 (0.12)	0.651 (0.11)	0.342 (0.14)	0.719 (0.09)	0.525 (0.12)	0.768 (0.13)	0.418 (0.24)
	80	0.548 (0.10)	0.118 (0.11)	0.759 (0.05)	0.398 (0.12)	0.821 (0.03)	0.572 (0.11)	0.881 (0.04)	0.606 (0.22)
	100	0.524 (0.14)	0.153 (0.16)	0.744 (0.08)	0.503 (0.13)	0.831 (0.05)	0.658 (0.08)	0.919 (0.02)	0.805 (0.08)
3	40	0.013 (0.02)	0 (0)	0.181 (0.09)	0.086 (0.05)	0.319 (0.05)	0.237 (0.07)	-	-
	60	0.058 (0.06)	0.010 (0.02)	0.267 (0.08)	0.136 (0.06)	0.394 (0.05)	0.305 (0.04)	0.286 (0.03)	0.021 (0.03)
	80	0.109 (0.08)	0.012 (0.02)	0.327 (0.14)	0.170 (0.10)	0.447 (0.17)	0.321 (0.13)	0.476 (0.08)	0.161 (0.11)
	100	0.160 (0.09)	0.016 (0.02)	0.412 (0.07)	0.218 (0.06)	0.546 (0.04)	0.391 (0.06)	0.584 (0.05)	0.224 (0.09)
4	40	0.113 (0.11)	0.075 (0.10)	0.291 (0.09)	0.240 (0.10)	0.374 (0.06)	0.378 (0.09)	-	-
	60	0.187 (0.15)	0.138 (0.09)	0.356 (0.08)	0.340 (0.09)	0.418 (0.05)	0.473 (0.07)	0.533	0.238
	80	0.312 (0.16)	0.198 (0.08)	0.470 (0.09)	0.413 (0.07)	0.516 (0.09)	0.533 (0.06)	0.617 (0.08)	0.338 (0.07)
	100	0.519 (0.08)	0.219 (0.07)	0.612 (0.11)	0.464 (0.07)	0.642 (0.12)	0.580 (0.06)	0.729 (0.05)	0.453 (0.04)

Table 1: Hypervolume Indicator averaged over 10 runs for different central parts of the Pareto front, budgets and number of objectives. The true Pareto front has an Hypervolume Indicator of 1.

m	$budget$	$\mathbf{R}^{0.1}$		$\mathbf{R}^{0.2}$		$\mathbf{R}^{0.3}$		\mathbf{R}^*	
		C-EHI	EHI	C-EHI	EHI	C-EHI	EHI	C-EHI	EHI
2	40	Inf	Inf	0.176 (0.09)	Inf	0.228 (0.05)	0.293 (0.20)	0.069	0.175
	60	0.095 (0.05)	Inf	0.109 (0.05)	0.204 (0.08)	0.133 (0.06)	0.184 (0.06)	0.066 (0.02)	Inf
	80	0.059 (0.02)	Inf	0.058 (0.01)	0.171 (0.05)	0.067 (0.02)	0.161 (0.07)	0.050 (0.01)	0.149 (0.05)
	100	0.067 (0.02)	Inf	0.059 (0.02)	0.138 (0.05)	0.055 (0.02)	0.118 (0.03)	0.048 (0.02)	0.109 (0.03)
3	40	Inf	Inf	0.455 (0.13)	0.518 (0.13)	0.531 (0.12)	0.500 (0.10)	-	-
	60	Inf	Inf	0.388 (0.11)	0.460 (0.11)	0.471 (0.13)	0.439 (0.06)	0.196 (0.03)	Inf
	80	0.238 (0.10)	Inf	0.256 (0.12)	0.361 (0.17)	0.339 (0.14)	0.356 (0.14)	0.181 (0.05)	Inf
	100	0.226 (0.05)	Inf	0.250 (0.05)	0.349 (0.06)	0.335 (0.08)	0.351 (0.07)	0.183 (0.05)	0.349 (0.08)
4	40	Inf	Inf	0.381 (0.05)	0.447 (0.12)	0.626 (0.07)	0.571 (0.07)	-	-
	60	0.280 (0.13)	Inf	0.334 (0.04)	0.359 (0.06)	0.587 (0.07)	0.512 (0.07)	0.197	0.233
	80	0.210 (0.06)	0.282 (0.06)	0.285 (0.05)	0.298 (0.04)	0.523 (0.08)	0.460 (0.06)	0.212 (0.04)	0.262 (0.08)
	100	0.158 (0.02)	0.266 (0.06)	0.236 (0.05)	0.277 (0.03)	0.468 (0.08)	0.430 (0.05)	0.257 (0.04)	0.291 (0.08)

Table 2: Inverted Generational Distance averaged over 10 runs for different central parts of the Pareto front, budgets and number of objectives. Lower values are better.

The average performance measures reported in Tables 1 to 3 confirm the behavior of the C-EHI algorithm already illustrated in Figure 23 for a typical run: mEI set to improve on the estimated center efficiently drives the algorithm towards the (unknown) central part of the real Pareto front. Table 1 summarizes test results expressed in terms of hypervolume improvements. In the most central part of the front ($w = 0.1$) C-EHI significantly surpasses the standard EHI. It is also remarkable that despite early GPs inaccuracies, the algorithm does not drift towards off-centered

m	$budget$	$\mathbf{R}^{0.1}$		$\mathbf{R}^{0.2}$		$\mathbf{R}^{0.3}$		Whole front		\mathbf{R}^*	
		C-EHI	EHI	C-EHI	EHI	C-EHI	EHI	C-EHI	EHI	C-EHI	EHI
2	40	Inf	Inf	0.033 (0.02)	Inf	0.033 (0.02)	0.121 (0.12)	0.033 (0.02)	0.076 (0.08)	0.014	0.078
	60	0.024 (0.02)	Inf	0.014 (0.01)	0.081 (0.04)	0.014 (0.01)	0.061 (0.03)	0.012 (0.01)	0.042 (0.03)	0.009 (0.01)	Inf
	80	0.010 (0.01)	Inf	0.008 (0)	0.062 (0.02)	0.007 (0)	0.052 (0.03)	0.006 (0)	0.032 (0.02)	0.003 (0)	0.044 (0.02)
	100	0.017 (0.02)	Inf	0.010 (0.01)	0.041 (0.02)	0.008 (0.01)	0.034 (0.02)	0.003 (0.01)	0.022 (0.02)	0.003 (0)	0.027 (0.02)
3	40	Inf	Inf	0.086 (0.07)	0.162 (0.07)	0.060 (0.03)	0.128 (0.07)	0.046 (0.03)	0.037 (0.02)	-	-
	60	Inf	Inf	0.037 (0.02)	0.116 (0.05)	0.023 (0.02)	0.083 (0.04)	0.019 (0.01)	0.021 (0.02)	0.039 (0.01)	Inf
	80	0.053 (0.04)	Inf	0.022 (0.02)	0.078 (0.05)	0.008 (0.01)	0.044 (0.03)	0.008 (0.01)	0.010 (0.01)	0.017 (0.01)	Inf
	100	0.044 (0.03)	Inf	0.023 (0.02)	0.065 (0.03)	0.004 (0.01)	0.042 (0.03)	0.004 (0.01)	0.008 (0.01)	0.008 (0.01)	0.053 (0.03)
4	40	Inf	Inf	0.016 (0.02)	0.023 (0.03)	0.016 (0.02)	0.010 (0.02)	0.012 (0.01)	0.004 (0.01)	-	-
	60	0.028 (0.04)	Inf	0.005 (0.01)	0.015 (0.02)	0.005 (0.01)	0.007 (0.02)	0.005 (0.01)	0 (0)	0	0
	80	0.008 (0.01)	0.019 (0.02)	0.001 (0)	0.005 (0.01)	0.001 (0)	0.004 (0.01)	0.001 (0)	0 (0)	0 (0)	0.010 (0.01)
	100	0 (0)	0.012 (0.01)	0 (0)	0.002 (0)	0 (0)	0.001 (0)	0 (0)	0 (0)	0 (0)	0.003 (0.01)

Table 3: ε -Indicator averaged over 10 runs for different central parts of the Pareto front, budgets and number of objectives. Lower values are better.

locations of the front. EHI outperforms C-EHI only with 4 objectives and $w = 0.3$, since in this case \mathcal{I}_w is not a restrictive central part in such dimension.

The IGD (Table 2) shows similar results. Notice that for at least one run, the classical EHI does not reach the $\mathcal{I}_{0.1}$ area in the two and three objective cases, even if 100 evaluations are allowed. In the 4 dimensional case, at least 80 iterations are needed. Again, the results show smaller distances between points in $\mathcal{P}_Y \cap \mathcal{I}_w$ and $\widehat{\mathcal{P}}_Y$ with C-EHI for 2 objectives, and when the restriction area is small. For 4 objectives and $w = 0.3$, EHI outperforms C-EHI, but in this case $\mathcal{I}_{0.3}$ is a quite large part of Y . Many solutions in $\mathcal{P}_Y \cap \mathcal{I}_{0.3}$ are thus far away from the area where C-EHI converges.

Test results expressed in terms of the ε -Indicator, which is a distance to the Pareto front, are provided in Table 3. In narrow central areas, C-EHI performs very well, meaning that the best point of $\widehat{\mathcal{P}}_Y \cap \mathcal{I}_w$ is close to $\mathcal{P}_Y \cap \mathcal{I}_w$. When considering the whole Pareto front, closeness to optimal solutions is improved using C-EHI with 2 and 3 objectives. The ε -Indicator with the whole front is similar to that with the restrictions to \mathcal{I}_w , meaning that the closest points to \mathcal{P}_Y have occurred in the central part. It is not necessarily the case for EHI. Many 0's occur in the last row of Table 3 where $m = 4$. The reason is that, with many objectives, the true Pareto front does not only contain points coming from NSGA-II but also from EHI or C-EHI optimizations.

Other indicators such as attainment times (average/median/worse number of iterations over the 10 experiments to reach some central objective values) confirmed the results reported above, but are not given here for reasons of brevity.

8 Conclusions

In this work, we have developed new concepts and have adapted existing Bayesian multi-objective optimization methods to enhance convergence to equilibrated solutions of a multi-objective optimization problem at severely restricted number of calls to the objective functions. The C-EHI algorithm proposed here is made of estimations of the Pareto center, maximizations of the mEI criterion and the optimal choice of a targeted central part of the Pareto front in accordance with

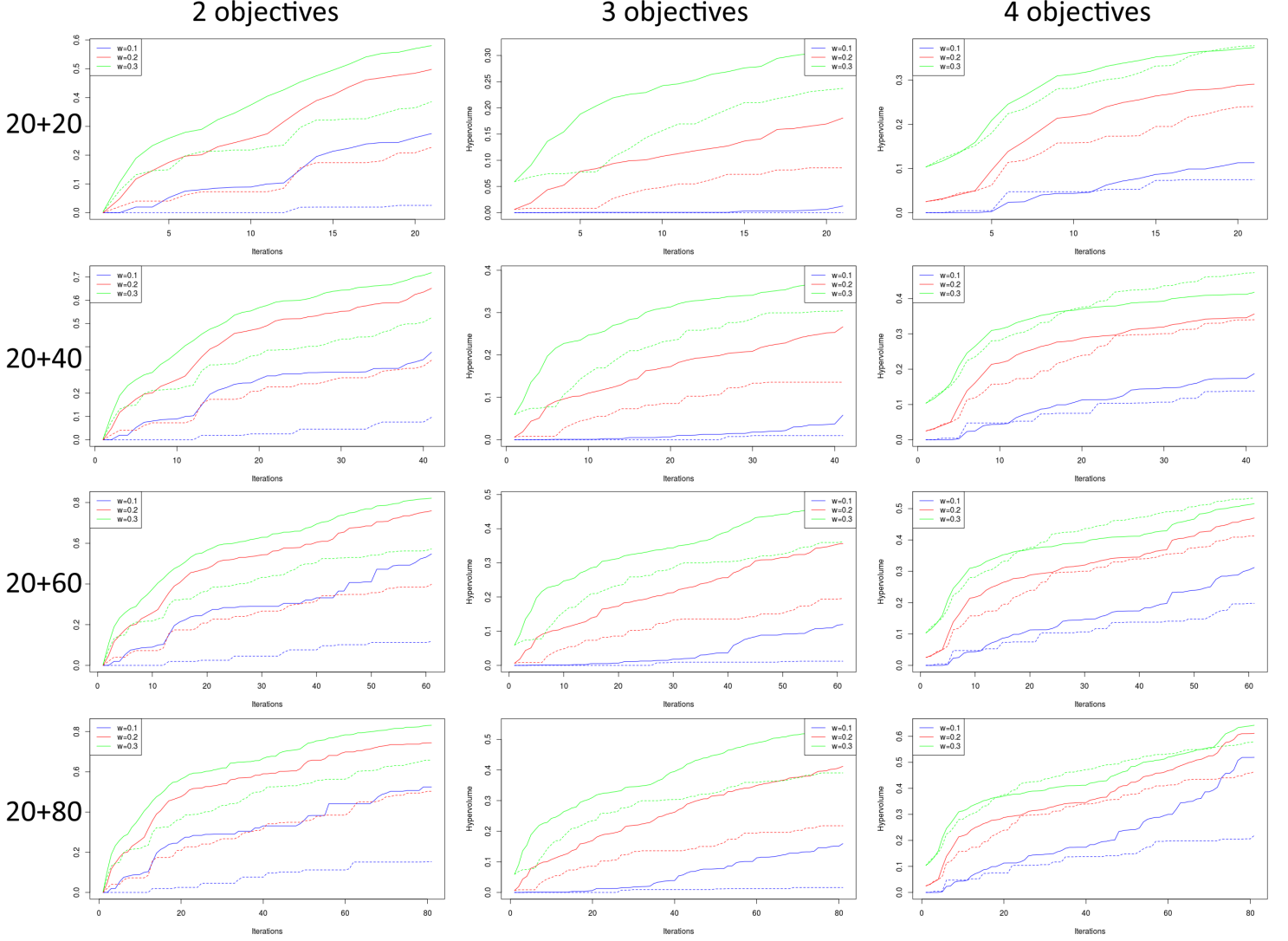


Figure 25: Mean Hypervolume Indicator for 2, 3 or 4 objectives (as columns) and total budgets of 40, 60, 80, 100 (as rows). The blue, red and green colors correspond to the improvement regions $\mathcal{I}_{0.1}$, $\mathcal{I}_{0.2}$ and $\mathcal{I}_{0.3}$, respectively. Dashed lines correspond to the standard EHI, continuous lines to the C-EHI algorithm.

the remaining budget. The C-EHI algorithm has shown better convergence to the center of the Pareto front than other state-of-the-art approaches. Continuations to this work should consider the effect of further increasing the number of objectives as the topology of Pareto fronts in high dimensional spaces remains largely unknown. It will also be important to describe and theoretically analyze other particular points of the Pareto front that might be then targeted with an appropriate

choice of the reference point and the mEI or EHI infill criterion.

Acknowledgements

The authors would like to acknowledge Philippe Solal for discussions about the center of the Pareto front, and Éric Touboul for his help for establishing geometric proofs related to the latter.

A Appendix: Nadir point estimation using Gaussian Processes

In the field of EMOA's, estimation procedures for extreme points, thus components of \mathbf{N} , have been proposed [15, 6]. In the Gaussian Processes framework, we look for \mathbf{x} 's that are likely to be extreme design points (Definition 3.3). Estimating the Nadir point through surrogates is a difficult task. When $m > 2$, the Nadir components come from extreme points that are not necessarily optimal in a single objective (cf. Definition 3.2). A straightforward estimation of the Nadir involves the knowledge of the whole Pareto front, as each component j of the Nadir point is dependent on the j -th objective function, but also on all other functions through the component-wise non-domination property of \mathbf{N} . However, the C-EHI algorithm only targets central solutions. With this algorithm, the GPs may not be accurate at non central locations of \mathcal{P}_Y . Using simulated values of the GPs instead of the kriging prediction should nonetheless reduce the impact of a potential inaccuracy as the latter is implicitly considered. Applying a step of mono-objective $f_j(\cdot)$ minimization (e.g. using EGO) might diminish this difficulty (at least for the \mathbf{I} estimation), at the expense of m costly evaluations of the computer code.

We now explain the proposed estimation approach. Extreme points have the property of being both *large* in the j -th objective and not dominated (ND). We are thus interested in \mathbf{x} 's with a high probability $\mathbb{P}(Y_j(\mathbf{x}) > a_j, \mathbf{Y}(\mathbf{x}) \text{ ND})$, for $j = 1, \dots, m$. A typical choice for a_j is the j -th component of the Nadir of the current Pareto front approximation, $\hat{\nu}_j^j$. Non-Domination refers to the current Pareto front approximation $\widehat{\mathcal{P}}_Y$. These events are not independent since $\mathbf{Y}(\mathbf{x})$ contains $Y_j(\mathbf{x})$. However, by conditioning on $Y_j(\mathbf{x}) > \hat{\nu}_j^j$, $\mathbb{P}(Y_j(\mathbf{x}) > \hat{\nu}_j^j, \mathbf{Y}(\mathbf{x}) \text{ ND}) = \mathbb{P}(\mathbf{Y}(\mathbf{x}) \text{ ND} | Y_j(\mathbf{x}) > \hat{\nu}_j^j) \times \mathbb{P}(Y_j(\mathbf{x}) > \hat{\nu}_j^j)$. The first part can be further simplified: to be non-dominated by $\widehat{\mathcal{P}}_Y$, a vector $\mathbf{z} \in \mathbb{R}^m$ with $z_j > \max_{\mathbf{y} \in \widehat{\mathcal{P}}_Y} y_j$ has to be non-dominated by $\widehat{\mathcal{P}}_Y$ with

regard to objectives $1, \dots, j-1, j+1, \dots, m$. Hence, $\mathbb{P}(\mathbf{Y}(\mathbf{x}) \text{ ND} | Y_j(\mathbf{x}) > \hat{\nu}_j^j) = \mathbb{P}(\mathbf{Y}(\mathbf{x}) \text{ ND}_{\setminus \{j\}})$ where $\text{ND}_{\setminus \{j\}}$ stands for non-domination omitting the objective j . Finally, the most promising candidates for generating extreme points of the Pareto front are those with great probability $\mathbb{P}(\mathbf{Y}(\mathbf{x}) \text{ ND}_{\setminus \{j\}}) \times \mathbb{P}(Y_j(\mathbf{x}) > \hat{\nu}_j^j)$.

Besides these candidates, a second scenario will lead to new extreme points. If $\mathbf{z} \in \mathbb{R}^m \preceq \hat{\nu}^j$ is obtained through simulations, $\hat{\nu}^j$ will no longer belong to the simulated Pareto front. Consequently, the j -th component of the Nadir point of the simulated front will also be modified in that case. When $m = 2$, the new $\hat{\nu}_j^j$ will be z_j , but this does not necessarily hold in higher dimensions.

In short, two events will lead to new extreme points: dominating the j -th current extreme point, $\{\mathbf{Y}(\mathbf{x}) \preceq \hat{\nu}^j\}$, or being both larger than it in j -th objective and ND with respect to the approximation front in the remaining objectives, $\{Y_j(\mathbf{x}) > \hat{\nu}_j^j, \mathbf{Y}(\mathbf{x}) \text{ ND}_{\setminus \{j\}}\}$. The areas corresponding

to these events are sketched with a 2D example in Figure 26. Being disjoint, the probability of the union of these events equals the sum. In the end, for estimating the j extreme points and by extension \mathbf{N} , the most promising candidates are those maximizing

$$\mathbb{P}(\mathbf{Y}(\mathbf{x}) \text{ ND}_{\setminus\{j\}}) \times \mathbb{P}(Y_j(\mathbf{x}) > \hat{\nu}_j^j) + \mathbb{P}(\mathbf{Y}(\mathbf{x}) \preceq \hat{\nu}^j), \quad (11)$$

for $j = 1, \dots, m$. $\mathbb{P}(\mathbf{Y}(\mathbf{x}) \text{ ND}_{\setminus\{j\}})$ is the probability of being non-dominated with respect to a $m - 1$ dimensional front (which is smaller than the restriction of $\widehat{\mathcal{P}}_{\mathbf{y}}$ to $\{1, \dots, m\} \setminus \{j\}$) and is the more computationally demanding term for a given \mathbf{x} . The other terms are univariate and product of univariate Gaussian CDF's, respectively.

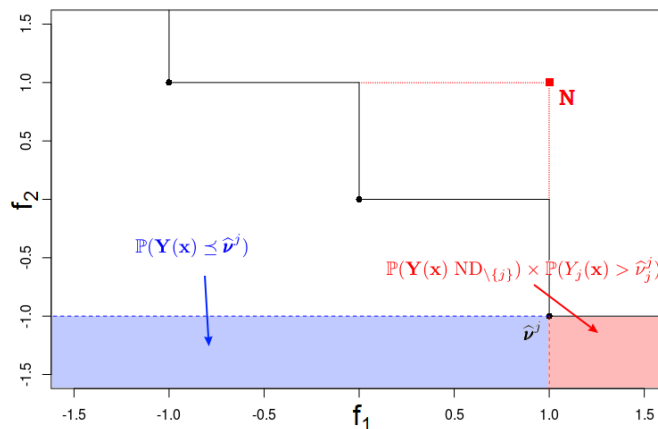


Figure 26: Areas leading to a new first component of the Nadir ($j = 1$). A point in the red zone (larger than the first extreme point in the first objective) or in the blue zone (dominating the current extreme point) becomes the new (first) extreme point, and therefore induces a modification of \mathbf{N} .

In the particular case of two objectives, the union of these events reduces to dominating $\hat{\nu}^j$ in all objectives but j , that is to say, in the other objective \bar{j} . This is equivalent to looking for candidates with lower $f_{\bar{j}}(\cdot)$, which has already been investigated when looking for candidates for estimating $I_{\bar{j}}$. Unfortunately, in a general m -dimensional case no simplification occurs. The set of candidates that are likely to dominate $\hat{\nu}^j$ in all objectives but j is included but not equal to the set of candidates likely to maximize (11), whose probabilities are respectively $\mathbb{P}(\mathbf{Y}(\mathbf{x}) \preceq_{\setminus\{j\}} \hat{\nu}^j)$ and $\mathbb{P}(\mathbf{Y}(\mathbf{x}) \text{ ND}_{\setminus\{j\}}) \times \mathbb{P}(Y_j(\mathbf{x}) > \hat{\nu}_j^j) + \mathbb{P}(\mathbf{Y}(\mathbf{x}) \preceq \hat{\nu}^j)$, as the latter encompasses more cases for producing new extreme points when $m > 2$. It is indeed possible to construct $\mathbf{z} \in \mathbb{R}^m$ such that $z_j > \nu_j^j$, $\mathbf{z} \text{ ND}_{\setminus\{j\}}$ and $\mathbf{z} \not\preceq_{\setminus\{j\}} \hat{\nu}^j$. Such a \mathbf{z} will become the j -th extreme point without dominating the previous j -th extreme point in objectives $\{1, \dots, m\} \setminus \{j\}$.

References

- [1] Anne Auger, Johannes Bader, Dimo Brockhoff, and Eckart Zitzler. Articulating user preferences in many-objective problems by sampling the weighted hypervolume. In *Proceedings of the 11th Annual conference on Genetic and evolutionary computation*, pages 555–562. ACM, 2009.

- [2] Anne Auger, Johannes Bader, Dimo Brockhoff, and Eckart Zitzler. Investigating and exploiting the bias of the weighted hypervolume to articulate user preferences. In *Proceedings of the 11th Annual conference on Genetic and evolutionary computation*, pages 563–570. ACM, 2009.
- [3] Anne Auger, Johannes Bader, Dimo Brockhoff, and Eckart Zitzler. Theory of the hypervolume indicator: optimal μ -distributions and the choice of the reference point. In *Proceedings of the tenth ACM SIGEVO workshop on Foundations of genetic algorithms*, pages 87–102. ACM, 2009.
- [4] Anne Auger, Johannes Bader, Dimo Brockhoff, and Eckart Zitzler. Hypervolume-based multi-objective optimization: Theoretical foundations and practical implications. *Theoretical Computer Science*, 425:75–103, 2012.
- [5] Slim Bechikh, Marouane Kessentini, Lamjed Ben Said, and Khaled Ghédira. Preference incorporation in evolutionary multiobjective optimization: a survey of the state-of-the-art. In *Advances in Computers*, volume 98, pages 141–207. Elsevier, 2015.
- [6] Slim Bechikh, Lamjed Ben Said, and Khaled Ghedira. Estimating Nadir point in multi-objective optimization using mobile reference points. In *Evolutionary computation (CEC), 2010 IEEE congress on*, pages 1–9. IEEE, 2010.
- [7] Julien Bect, Ling Li, and Emmanuel Vazquez. Bayesian subset simulation. *SIAM/ASA Journal on Uncertainty Quantification*, 5(1):762–786, 2017.
- [8] Mickael Binois and Victor Picheny. GPareto: An R package for Gaussian-process based multi-objective optimization and analysis.
- [9] Mickaël Binois. *Uncertainty quantification on Pareto fronts and high-dimensional strategies in Bayesian optimization, with applications in multi-objective automotive design*. PhD thesis, École Nationale Supérieure des Mines de Saint-Etienne, 2015.
- [10] Dimo Brockhoff, Johannes Bader, Lothar Thiele, and Eckart Zitzler. Directed multiobjective optimization based on the weighted hypervolume indicator. *Journal of Multi-Criteria Decision Analysis*, 20(5-6):291–317, 2013.
- [11] Dimo Brockhoff, Tea Tusar, Dejan Tusar, Tobias Wagner, Nikolaus Hansen, and Anne Auger. Biobjective performance assessment with the COCO platform. *CoRR*, abs/1605.01746, 2016.
- [12] Carlos A Coello Coello and Nareli Cruz Cortés. Solving multiobjective optimization problems using an artificial immune system. *Genetic Programming and Evolvable Machines*, 6(2):163–190, 2005.
- [13] Noel Cressie. *Statistics for spatial data*. John Wiley & Sons, 2015.
- [14] Kalyanmoy Deb. *Multi-objective optimization using evolutionary algorithms*, volume 16. John Wiley & Sons, 2001.
- [15] Kalyanmoy Deb, Kaisa Miettinen, and Shamik Chaudhuri. Toward an estimation of Nadir objective vector using a hybrid of evolutionary and local search approaches. *IEEE Transactions on Evolutionary Computation*, 14(6):821–841, 2010.

- [16] Kalyanmoy Deb, Amrit Pratap, Sameer Agarwal, and Tamt Meyarivan. A fast and elitist multiobjective genetic algorithm: NSGA-II. *IEEE transactions on evolutionary computation*, 6(2):182–197, 2002.
- [17] Kalyanmoy Deb and J Sundar. Reference point based multi-objective optimization using evolutionary algorithms. In *Proceedings of the 8th annual conference on Genetic and evolutionary computation*, pages 635–642. ACM, 2006.
- [18] Michael Emmerich, Nicola Beume, and Boris Naujoks. An EMO algorithm using the hypervolume measure as selection criterion. In *International Conference on Evolutionary Multi-Criterion Optimization*, pages 62–76. Springer, 2005.
- [19] Michael Emmerich, André Deutz, and Jan Willem Klinkenberg. Hypervolume-based expected improvement: Monotonicity properties and exact computation. In *Evolutionary Computation (CEC), 2011 IEEE Congress on*, pages 2147–2154. IEEE, 2011.
- [20] Michael Emmerich, Kyriakos Giannakoglou, and Boris Naujoks. Single-and multiobjective evolutionary optimization assisted by Gaussian random field metamodels. *IEEE Transactions on Evolutionary Computation*, 10(4):421–439, 2006.
- [21] Paul Feliot. *Une approche Bayésienne pour l’optimisation multi-objectif sous contraintes*. PhD thesis, Université Paris-Saclay, 2017.
- [22] Carlos M Fonseca and Peter J Fleming. Multiobjective optimization and multiple constraint handling with evolutionary algorithms. I. A unified formulation. *IEEE Transactions on Systems, Man, and Cybernetics-Part A: Systems and Humans*, 28(1):26–37, 1998.
- [23] David Ginsbourger, Rodolphe Le Riche, and Laurent Carraro. Kriging is well-suited to parallelize optimization. In *Computational Intelligence in Expensive Optimization Problems*, pages 131–162. Springer, 2010.
- [24] John H Halton. On the efficiency of certain quasi-random sequences of points in evaluating multi-dimensional integrals. *Numerische Mathematik*, 2(1):84–90, 1960.
- [25] Markus Hartikainen, Kaisa Miettinen, and Margaret M Wiecek. PAINT: Pareto front interpolation for nonlinear multiobjective optimization. *Computational optimization and applications*, 52(3):845–867, 2012.
- [26] Hisao Ishibuchi, Yasuhiro Hitotsuyanagi, Noritaka Tsukamoto, and Yusuke Nojima. Many-objective test problems to visually examine the behavior of multiobjective evolution in a decision space. In *International Conference on Parallel Problem Solving from Nature*, pages 91–100. Springer, 2010.
- [27] Shinkyu Jeong and Shigeru Obayashi. Efficient Global Optimization (EGO) for multi-objective problem and data mining. In *Evolutionary Computation, 2005. The 2005 IEEE Congress on*, volume 3, pages 2138–2145. IEEE, 2005.
- [28] Donald R Jones. A taxonomy of global optimization methods based on response surfaces. *Journal of global optimization*, 21(4):345–383, 2001.

- [29] Donald R Jones. Large-scale multi-disciplinary mass optimization in the auto industry. In *MOPTA 2008 Conference (20 August 2008)*, 2008.
- [30] Donald R Jones, Matthias Schonlau, and William J Welch. Efficient Global Optimization of expensive black-box functions. *Journal of Global optimization*, 13(4):455–492, 1998.
- [31] Ehud Kalai and Meir Smorodinsky. Other solutions to Nash’s bargaining problem. *Econometrica: Journal of the Econometric Society*, pages 513–518, 1975.
- [32] Andy J Keane. Statistical improvement criteria for use in multiobjective design optimization. *AIAA journal*, 44(4):879–891, 2006.
- [33] Joshua Knowles. ParEGO: A hybrid algorithm with on-line landscape approximation for expensive multiobjective optimization problems. *IEEE Transactions on Evolutionary Computation*, 10(1):50–66, 2006.
- [34] Joshua Knowles and David Corne. On metrics for comparing nondominated sets. In *Evolutionary Computation, 2002. CEC’02. Proceedings of the 2002 Congress on*, volume 1, pages 711–716. IEEE, 2002.
- [35] Longmei Li, Iryna Yevseyeva, Vitor Basto-Fernandes, Heike Trautmann, Ning Jing, and Michael Emmerich. An ontology of preference-based multiobjective evolutionary algorithms. *arXiv preprint arXiv:1609.08082*, 2016.
- [36] Wudong Liu, Qingfu Zhang, Edward Tsang, Cao Liu, and Botond Virginas. On the performance of metamodel assisted MOEA/D. In *International Symposium on Intelligence Computation and Applications*, pages 547–557. Springer, 2007.
- [37] Jonas Mockus. On Bayesian methods for seeking the extremum. In *Optimization Techniques IFIP Technical Conference*, pages 400–404. Springer, 1975.
- [38] Ilya Molchanov. *Theory of Random Sets*. Probability and Its Applications. Springer London, 2005.
- [39] Max D Morris and Toby J Mitchell. Exploratory designs for computational experiments. *Journal of statistical planning and inference*, 43(3):381–402, 1995.
- [40] James Parr. *Improvement criteria for constraint handling and multiobjective optimization*. PhD thesis, University of Southampton, 2013.
- [41] Victor Picheny. Multiobjective optimization using Gaussian process emulators via stepwise uncertainty reduction. *Statistics and Computing*, 25(6):1265–1280, 2015.
- [42] Wolfgang Ponweiser, Tobias Wagner, Dirk Biermann, and Markus Vincze. Multiobjective optimization on a limited budget of evaluations using model-assisted S-metric selection. In *International Conference on Parallel Problem Solving from Nature*, pages 784–794. Springer, 2008.
- [43] Carl Edward Rasmussen and Christopher KI Williams. *Gaussian Processes for Machine Learning*. The MIT Press, 2006.

- [44] Olivier Roustant, David Ginsbourger, and Yves Deville. DiceKriging, DiceOptim: Two R packages for the analysis of computer experiments by kriging-based metamodeling and optimization. 2012.
- [45] Jerome Sacks, William J Welch, Toby J Mitchell, and Henry P Wynn. Design and analysis of computer experiments. *Statistical science*, pages 409–423, 1989.
- [46] Thomas J Santner, Brian J Williams, and William I Notz. *The design and analysis of computer experiments*. Springer Science & Business Media, 2013.
- [47] Il’ya Meerovich Sobol’. On the distribution of points in a cube and the approximate evaluation of integrals. *Zhurnal Vychislitel’noi Matematiki i Matematicheskoi Fiziki*, 7(4):784–802, 1967.
- [48] Michael L Stein. Large sample properties of simulations using latin hypercube sampling. *Technometrics*, 29(2):143–151, 1987.
- [49] Michael L Stein. *Interpolation of spatial data: some theory for kriging*. Springer Science & Business Media, 2012.
- [50] Joshua Svenson. *Computer experiments: Multiobjective optimization and sensitivity analysis*. PhD thesis, The Ohio State University, 2011.
- [51] Joshua Svenson and Thomas J Santner. Multiobjective optimization of expensive black-box functions via expected maximin improvement. *The Ohio State University, Columbus, Ohio*, 32, 2010.
- [52] Tobias Wagner, Michael Emmerich, André Deutz, and Wolfgang Ponweiser. On expected-improvement criteria for model-based multi-objective optimization. In *International Conference on Parallel Problem Solving from Nature*, pages 718–727. Springer, 2010.
- [53] Kaifeng Yang, Andre Deutz, Zhiwei Yang, Thomas Back, and Michael Emmerich. Truncated expected hypervolume improvement: Exact computation and application. In *Evolutionary Computation (CEC), 2016 IEEE Congress on*, pages 4350–4357. IEEE, 2016.
- [54] Kaifeng Yang, Michael Emmerich, André Deutz, and Carlos M Fonseca. Computing 3-D expected hypervolume improvement and related integrals in asymptotically optimal time. In *International Conference on Evolutionary Multi-Criterion Optimization*, pages 685–700. Springer, 2017.
- [55] Kaifeng Yang, Daniel Gaida, Thomas Bäck, and Michael Emmerich. Expected hypervolume improvement algorithm for PID controller tuning and the multiobjective dynamical control of a biogas plant. In *Evolutionary Computation (CEC), 2015 IEEE Congress on*, pages 1934–1942. IEEE, 2015.
- [56] Kaifeng Yang, Longmei Li, André Deutz, Thomas Back, and Michael Emmerich. Preference-based multiobjective optimization using truncated expected hypervolume improvement. In *Natural Computation, Fuzzy Systems and Knowledge Discovery (ICNC-FSKD), 2016 12th International Conference on*, pages 276–281. IEEE, 2016.
- [57] Qingfu Zhang, Wudong Liu, Edward Tsang, and Botond Virginas. Expensive multiobjective optimization by MOEA/D with Gaussian process model. *IEEE Transactions on Evolutionary Computation*, 14(3):456–474, 2010.

- [58] Eckart Zitzler. Evolutionary algorithms for multiobjective optimization: Methods and applications. 1999.
- [59] Eckart Zitzler, Dimo Brockhoff, and Lothar Thiele. The hypervolume indicator revisited: On the design of Pareto-compliant indicators via weighted integration. In *International Conference on Evolutionary Multi-Criterion Optimization*, pages 862–876. Springer, 2007.
- [60] Eckart Zitzler, Lothar Thiele, Marco Laumanns, Carlos M Fonseca, and Viviane Grunert Da Fonseca. Performance assessment of multiobjective optimizers: An analysis and review. *IEEE Transactions on evolutionary computation*, 7(2):117–132, 2003.